Morphological Design for Block Copolymer/Homopolymer Based Thin Film Blend Systems

by

Junnan Zhao

A dissertation submitted in partial fulfillment
of the requirements for the degree of
Doctor of Philosophy
(Materials Science and Engineering)
in the University of Michigan
2016

Doctoral Committee:

Professor Peter *F.* Green, Chair
Professor Richard E. Robertson
Associate Professor Pramod Sangi Reddy
Associate Professor Anish Tuteja

To my family

ACKNOWLEDGMENTS

It's really an exciting moment to express my deepest gratitude to many people who have given me help and support on the journey of pursuing this doctoral degree. Without their warmhearted support and generous help, I would never have been able to complete my study and have this dissertation.

First and foremost, I would like to offer my sincere thanks to my advisor Professor Peter *F.* Green. I feel tremendous fortune to have such a great advisor who continuously encouraged me and gave me patient guidance throughout my Ph.D. years. I was always having freedom to carry out the research projects I was interested in and meanwhile I felt welcome to talk with him whenever I got stuck into the projects. His invaluable insights and tireless guidance motivated me to give my best. No words could possibly express my thanks to him and I believe many great things I learned from him will exert a lasting impact on my future career.

I would also like to thank my committee members, Professor Richard Robertson, Associate Professor Anish Tuteja and Associate Professor Pramod Sangi Reddy. They were always very responsive when I scheduled my preliminary exam, data meeting and defense with them. I appreciated the precious time they spent in getting to know my research and giving insightful comments. Professor Tuteja raised critical questions on my polymer

nanocomposite projects during my data meeting, which helped me think hard to elaborate my work. In addition, I want to thank Professor Robertson and Professor Tuteja for their excellent teaching on the courses of *polymeric materials* and *polymer physics* respectively which were valuable for my research.

Next, my appreciation will go to my current and previous Green group members, including Jojo Amonoo, Anton Li, Ban Dong, Kyle Johnson, Ravi Sharma, Jill Wenderott, Dr. Aaron C. Tan, Dr. Peter Chung, Dr. Hengxi Yang, Dr. Bingyuan Huang, Dr. Bradley R. Frieberg, Dr. Chelsea X. Chen, Dr. Carl McIntyre and Dr. Emmanouil Glynos. Because of them I never felt bored working in the lab. The group had a great working environment in which group members were supportive and collaborative. They never showed hesitation to lend a hand. Among all group members, I especially thank Chelsea who trained me transmission electron microscopy and nanoparticle synthesis when I was new to the group. Jenny, Bingyuan, Brad and Hengxi were also my teachers for various lab characterization techniques. I also thank Chelsea and Hengxi for their fruitful discussion on the polymer nanocomposite projects.

I would like to acknowledge EMAL staff Dr. Kai Sun for his tremendous assistance in electron microscopes and UCSB scientist Dr. Tom Mates for his help on secondary ion mass spectroscopic measurement. I also want to send my gratefulness to Dr. Gerogios Sakellariou from University of Athens, Greece who synthesized star-shaped polymers. Their tremendous help made contributions to my research and my dissertation.

I also want to thank the staff members of my department, Materials Science and Engineering, especially our graduate coordinator Renee Hilgendorf for her administrative support throughout my Ph.D. years.

Finally, I must express my greatest thanks to my family and friends. Although my family are thousands of miles away from me, their forever love and unconditional support make me to move on to the position where I am. It was of great power and strength to go through hardship when I knew they are always there to support me. Apart from endless support of distant family, many friends I made in Ann Arbor kept me away from loneness and stress. Being together with them, I had tons of joyful moments when I looked back to my graduate life.

TABLE OF CONTENTS

LIST OF FIGURES

LIST OF TABLES

LIST OF APPENDICES

ABSTRACT

Polymer nanocomposites (PNCs) are created by incorporating nanoparticles (NPs) into polymer hosts. The properties of PNCs are determined by various intermolecular interactions and associated morphologies. The Precise control of morphologies and in particular spatial distributions of NPs in PNCs remains an important challenge; in thin films, the presence of interfaces places the additional constraint to control NP locations. These limit potential applications of PNCs. Research in this area has been devoted to bulk single polymer component PNCs: NPs in homopolymers and NPs in diblock copolymers (BCP). Research on thin films or multi polymer components PNCs remains limited despite the potential technological impact. In this dissertation, we designed nano-scale morphologies for thin film BCP/homopolymer blend based systems: (1) applying morphology design rules to create various NP spatial distributions in thin film BCP/homopolymer blends; (2) investigating phase behaviors of potential PNC polymer hosts, thin film BCP/star-shaped homopolymer blends.

We achieved the control of NP distributions in a mixture of BCP polystyrene-b-poly (2-vinylpyridine) (PS-b-P2VP) with homopolymer polystyrene (PS), in which PS-b-P2VP formed micelles composed of an inner core of P2VP block and an outer corona of PS block. P2VP grafted NPs (P2VP-NPs) were encapsulated within P2VP micelle cores and each

micelle contained one or no NP. In the case of PS grafted NPs (PS-NPs), prudent choices of grafted chain lengths and NP sizes enabled us to control NP locations, ranging from preferentially segregating to interfaces (free surface or/and substrate) to primarily locating on the surface of micelle cores. The competing enthalpic and entropic interactions dictate the various morphological structures that are not achievable in the single polymer component PNCs.

Following that we showed phase behaviors of thin film PS-b-P2VP/star-shaped PS blends could be tailored by the functionality and arm length of star-shaped PS due to its topology and associated entropy effects. The system, in which PS-b-P2VP also formed micelles, exhibited miscibility or phase separation of micelles in star-shaped PS. In the soft colloid-like star PS, close-packed micelles segregated toward the substrate, which is not achieved in the linear PS hosts. The BCP/star-shaped polymer system would increase the "template" available to organize NPs.

CHAPTER 1.
INTRODUCTION

1.1. Motivation and Research Objectives

Polymer nanocomposites (PNCs) comprise a class of technologically important hybrid materials in which nanofillers are incorporated into the polymer hosts. The nanoafillers are typically graphene, carbon nanotube, clay and nanoparticles. With addition of a small amount of nanofillers, PNCs have been shown to exhibit mechanical, electrical, optical and thermal properties superior to those of the polymer host.[1-7] Such property changes render PNCs useful for a wide range of applications in packaging, coating, automotive, sensors and biomedical science, based on the functionalities of the polymer host and nanofillers.

Despite over three decades of research in PNCs, there remain a number of challenging issues that may hinder the widespread use of PNCs. First, theories used to describe the conventional composites fail to predict the unusual property changes of PNCs even with a low concentration of nanofillers. This can be attributed to that the high surface area to volume ratio of nanofillers magnifies polymer/nanofiller interfacial regions where the properties differ from the bulk polymer. Second, experimentally, it is difficult to control the

complex morphologies (miscibility, phase separation or other controlled morphologies) which are largely dictated by competing energetic interactions like nanofiller-polymer interactions and nanofiller-nanofiller interactions. To resolve the above-mentioned issues and furthermore to achieve desired PNC properties, it is essential to gain insight into the fundamental energetic interactions that control nanofiller distribution in polymer hosts.

In thin films, the related issue is the need to understand even subtle morphological changes induced by interfaces and thus in turn to understand the change of properties of PNCs.[8] Since many emerging technical applications such as coatings,[9] optical sensors[5] and organic data storage devices,[10] require PNCs confined in thin film geometries, it is very crucial to understand and to control nanofiller distribution throughout the films and particularly near interfaces.

To this end, our goal is to gain control of nano-scale morphology in thin film PNCs and to establish morphological design rules for desired PNC properties. This can be obtained from a fundamental understanding of various collective entropic and enthalpic intermolecular interactions between polymer hosts and nanoparticles (NPs). Research in this field has been primarily devoted to understanding NP distribution in bulk single component polymer hosts like homopolymers or BCPs. In this dissertation, we investigate NP organization in thin film homopolymer/BCP polymer blends. In this system, we focus on polymer chain tethered nanoparticles. BCP chains, as a minor component form micelles throughout the homopolymer hosts as well as a layer of brush onto the substrate and different scenarios involving the spatial distribution of NPs occur under specific conditions. In chapter 2, specially functionalized NPs are shown to be encapsulated within the micelle cores and the effect of NP encapsulation on the formation and organization of micelles is also discussed. In chapter 3, we further discuss the spatial control of NP locations in terms

of size and grafted chain length of NPs, which is characterized by the morphological diagram. By carefully selecting the conditions, NPs might "decorate" the micelles or segregate to the external interfaces. In chapter 4, we explore the phase behaviors of a new class of polymer blend hosts by changing the linear homopolymers to star-shaped homopolymers in the polymer blends. The BCP chains, as a minor component also form micelles in star-shaped polymer thin films. The tailored phase behaviors of BCP/star-shaped polymer blend thin films are illustrated by tuning number of arms and arm lengths of star-shaped polymers. This new class of polymer blends is anticipated to serve as a template for NP organization.

The remaining parts of this chapter are intended to provide the background information and the context of the work described in the following chapters.

1.2. Overview of Polymer Nanocomposites

We begin the discussion with the morphology of NP/homopolymer mixtures followed by that of NP/BCP mixtures. In the context of this research, our discussion here will be restricted to the PNC systems containing polymer grafted NPs. The grafting densities ∑ of NPs are sufficiently high so that particle core-core attractions are screened.

1.2.1. Nanoparticles in homopolymer hosts: from bulk to thin film

The NP organization throughout the homopolymer is largely dictated by a complex interplay of enthalpic and entropic interactions between the grafted chains and host chains. There are a number of factors affecting the NP organization in homopolymer hosts, including chemistries of the grafted chains and the homopolymers, the degrees of

polymerization of the grafted chain N, and of the polymer host P, $\sum$ and the nanoparticle size R.[7,8,11]

In the simplest PNC system where the grafted polymer is chemically identical to the matrix polymer (i.e., the Flory-Huggin interaction parameter $\chi \approx 0$), there is no enthalpic interaction. In such cases, the NP organization in the host is primarily determined from the entropic effect pertaining to the grafted polymers and the host chains. It is well known from theoretical studies on interpenetrations of a polymer melt onto the polymer brushes.[12] Under the condition when host chains completely penetrate the brushes, there is a favorable interaction between the polymer melt and the polymer brushes; it is referred to "wet brush" regime in which NPs tend to disperse. In contrast, the condition under which host chains are expelled from the brushes or only penetrate at the outer region of the brushes is called "dry brush", accompanied by unfavorable interactions between host chains and grafted chains; this may lead to NP aggregation. Using scaling theory and strong segregation theory calculations, Leibler and his coworkers predicted that the transition from "wet brush" to "dry brush" occurs when $\Sigma N^{1/2} > (P/N)^{-2}$ provided $P/N<1$ and $\Sigma N^{1/2} = 1$ if $P/N>1$.[12] Subsequent self-consistent field theory (SCFT) studies by Matsen and coworkers showed that there are always attractive interactions between opposing brushes.[13] Nevertheless, the strength of the attraction decreases rapidly with increasing N/P and thus it's possible to have regimes of dispersion and aggregation which depend on Σ and P/N.

PNC systems in which the grafted chains and host chains are of different chemistries are also studied. In such systems, enthalpic interactions need to be considered. Leibler and Borukhov used scaling theory to examine the case of negative χ ($\chi < 0$) in which there are favorable enthalpic interactions between the grafted polymers and the hosts.[14] Their results

suggest that the condition for dispersion is extended to the long chains. Another study by Ryu, Ganesan and coworkers considered the case of positive χ ($\chi > 0$) in which the polymer melt exhibits unfavorable interactions with the brush.[15] The brush molecular weight dependent dewetting behavior was shown, similar to that expected for "dry brush" condition when $\chi \approx 0$, indicating a dominance of entropic effects.

The discussion in the previous part is based on results obtained from the flat grafted polymers, the curvature effect becomes significant when the grafted polymer chains are on the surface of small NPs, $R < N^{1/2}a$ (a is the segmental length).[16] The surface curvature of NPs increases with decreasing R. For a constant grafting density, the higher the curvature is, the less the grafted chains are stretched. As a consequence, the interaction between particles are expected to be weakened and the host chains tend to intermix with the grafted chains. A series of theoretical work demonstrated the curvature effect on the interaction of host chains with grafted chains.[17-20] Their studies showed the existence of repulsive interactions between two brushes coated spheres. In addition, NP dispersion is expected to be favorable for small particles since the translational entropy $F_{trans} \sim (\varphi/R^3)\ \ln\varphi$ (φ is volume fraction of NPs) increases with decreasing R.[21,22]

The foregoing discussion summarizes the interaction between polymer grafted NPs and host chains that occurs in bulk systems. In thin films, the interaction of constituents within PNCs with interfaces tends to alter morphologies from their bulk analogues. In an athermal system ($\chi \approx 0$), NPs exhibit a tendency to segregate to interfaces, including the free surface and the substrate due to a number of effects. Theoretical work by McGarrity and coworkers suggests that the free host chains gain conformational entropy by migrating away from interfaces.[23,24] It has been shown that the surface free energy/area gain $F_{ch} = \alpha k_B T (4V_{NP}/V_S R^2)$, where α is the number of degrees of freedom a polymer segment gains due to

migrating away from the interfaces, V_{NP} is the volume of a NP and V_S is the volume of a statistical segment. Grafted NPs segregating to the interfaces have additional entropy gains because the tethered chains suffer less entropy loss than the free host chains. When the nanoparticles become small or have long grafted chains such that $R < N^{1/2}a$, the structure of the NP starts resembling that of a star polymer. Archer and coworkers has shown surface enrichment of multi-arm star-shaped molecules in their mixture with linear analogues due to entropic effects.[25] Another driving force for interfacial segregation is van der Waals interaction between the substrate and NPs, particularly for large NPs. These interaction potential scales with ~R/(l+d), where l is the brush layer thickness and d is the distance between the brush surface and the substrate.[26] The interaction occurs on the length scale of a few nanometers. Van der Waals interactions diminish rapidly with decreasing NP size and increasing grafted chain length.

Meli et al. were the first to show that morphologies of athermal thin film NPs/homopolymer mixtures can be readily tailored through control of P/N and R.[27] A transition from miscibility to interfacial segregation occurred by increasing size of NP from R = 1nm to R = 2.5 nm when P/N >> 1 and N is small. For the fixed NP size of R = 2.5 nm and the fixed grafted chain length of N=480, by varying P/N ratios from 0.26 to 18, the different extent of intermixing between host chains and grafted chains leads to miscibility or phase separation. Subsequent detailed study by Kim on this athermal system developed a phase diagram in terms of P/N vs. N in which three regimes have been identified, including complete phase separation, interfacial segregation and miscibility.[28] Following this athermal system, Chen established a phase diagram as a function of P/N and curvature of NPs for the PNC system in which there is negative χ between grafted chains and host chains($\chi < 0$).[29]

The more dispersed NP for increasing values of N/P is associated with favorable enthalpic interactions between host chains and brush chains.

Overall, these studies have confirmed the interactions between the host chains and grafted chains and also demonstrated the subtle effect of interfaces present in thin films on NP distributions. These background information can be applied to our system of NPs in thin film homopolymer/BCP mixtures in Chapter 3 under conditions in which the intermolecular interaction between NPs and BCP chains becomes very weak or negligible.

1.2.2. Nanoparticles in diblock copolymer hosts: from bulk to thin film

The use of BCPs to organize NPs continues to garner much attention due to the fact that BCP chains composed of immiscible blocks can self-organize into long-range order structures of different geometries, including spherical, cylindrical, bicontinuous and lamellar domains.[30-32] These ordered structures and corresponding domain sizes are determined by BCP composition *f* (volume fraction of one block), χ between two immiscible blocks and the degree of polymerization of BCP. The overall enthalpic and entropic interactions between NPs and BCPs determines the overall morphology of NP/BCP systems. Grafting polymer chains on the surface of NPs is an effective strategy to control NP-polymer interactions.

The chemical nature of grafted chains, grafted chain lengths, grafting density, NP size and NP concentration directly influence the NP distribution in BCPs, which has been addressed by both theoretical and experimental work.[22,33-35] Depending on the chemistry of grafted chains, NPs can be selective to one particular domain. Such selective particles tend to segregate to the particular domain with which they are compatible. The grafting density of NPs can change the selectivity (compatibility) of NPs with respect to the particular domain, leading to a shift of NP locations from the interior of the selective domain to the interfacial

regions of two domains.[36-38] For example, PS grafted AuNPs in PS-b-P2VP matrix with lamellar structures, below some critical grafting density ($\sum$ < 2.36 chains/nm^2 for N = 14), preferred to reside at the interfaces of PS/P2VP blocks because NP core-P2VP block favorable enthalpic interaction dominated. When $\sum$ > 3.97 chains/nm^2, grafted PS-PS block entropic interaction dominated; thus, the NPs became selective to the PS blocks and located in the interior of the PS domains.[37] The critical $\sum$ decreased with increasing grafted chain length since longer grafted chain length can effectively screen the core-P2VP interactions.

The effect of NP size and concentration on NP locations will be discussed. For small particles (with ratio of NP size R over the BCP domain size, being less than 0.2), they preferentially locate within one domain or at the interface of two blocks since the gain in translational entropy dominates over the loss of conformational entropy of polymer chains. On the other hand, relatively larger particles (R/L>0.3) preferentially segregate to the center of appropriate domain in order to minimize the conformational entropy loss of polymer chains.[39] At a fixed R/L ratio, it is found that the amount of PS grafted AuNPs located at the center of PS domains of PS-b-P2VP BCP increased with NP concentration as suggested by narrow Gaussian distribution profile of NPs in PS domains.[40] Upon increasing NP concentration, the loss of conformational entropy throughout the PS domain cannot be compensated by the translational entropy gain. Therefore, large amount of NPs migrating to the center of PS domains upon increasing NP concentration can minimize the conformational entropy loss of polymer chains due to stretching. In addition, sufficiently high NP concentration can result in a morphological transition of the overall system. The coexistence of several different morphologies was found in the PS grafted NP/ PS-b-P2VP system due to variation in the local concentration of NPs.[41]

The foregoing discussion in this subsection highlights theoretical and experimental development on the morphologies of NP/BCP mixtures in the limit of bulk systems. In thin films, interfacial interactions of BCPs and NPs place the additional influence on the morphologies of NP/BCP thin films. Theoretical study by Lee et al., in NP/BCP mixtures confined between two hard walls reveals that a large amount of NPs segregated to the hard walls due to depletion attraction.[42] This point has been confirmed by subsequent theoretical studies.[43,44] Experimental studies also observed interfacial segregation of NPs towards the substrate or/and the free surface upon annealing.[45] In addition, the selectivity of the substrate to two blocks of BCPs can be used to direct the domain orientation for NP templating. For example, in the non-selective substrate, lamellar structures are well known to orient perpendicular to the substrate while in the selective substrate, they orient parallel to the substrate with alternating layers of two blocks. With an optimal film thickness, one can easily achieve the alternating layers with NPs.[46] When the films are not of an optimal thickness, the islands or holes are formed by accommodation of defect formation, e.g. edge dislocations. In such case, edge dislocations direct the locations of NPs since the chains that comprise the dislocations undergo less stretching and therefore gain conformational entropy by accommodating NPs.[47]

More theoretical and experimental studies are important to understand the morphologies of NP/BCP thin film mixtures. These background information will be helpful to understand the parts of this dissertation: (1) in chapter 2, the effect of NP encapsulation on the BCP micelle formation and organization in thin film homopolymer and (2) in chapter 3, rationales behind the phenomenon of NPs decorating BCP micelles in homopolymer thin films.

1.3. Diblock Copolymer/Homopolymer based Thin Film Blend Systems Studied in this Work

During the last three decades, most of studies in PNC thin films focused on single component homopolymer hosts or BCPs, as discussed in the previous sections. However, few studies have explored thin film polymer blends as PNC matrices. Thin film polymer blends exhibit unique surface properties and morphological behaviors which can be useful for various applications, smart coating, wetting, lubricant and biomedical use. In the following subsection, we will introduce the multi-component polymeric systems studied in this work.

1.3.1. Diblock copolymer/homopolymer thin films and nanoparticles in thin film diblock copolymer/homopolymer blends

When BCP chains are dissolved into a selective solvent (e.g. good solvent for one of the blocks) micelles are known to form in this selective solvent assuming that BCP concentration is above critical micelle concentration.[48] This fact also applies to the case in which the selective solvent is replaced with homopolymer of identical chemistry to one of the blocks. For example, the system contains BCP A-b-B/homopolymer A mixtures. To minimize the unfavorable enthalpic interaction between B block and homopolymer A, BCP as a minor component tends to self-assemble into micelles of various shapes, including spherical, cylindrical, lamellar and vesicle micelles.[49] The structure of micelles is determined by the degrees of polymerization of block A and block B, N_A and N_B respectively, the degree of polymerization of homopolymer P, χ between A and B and BCP concentration.

Recently our group studied morphologies of PS-b-P2VP/PS thin film mixtures in which the minor component PS-b-P2VP self-assembled into spherical micelles with an inner core of P2VP block and an outer corona of PS block throughout homopolymer PS hosts.[50] Micelle core size increased with increasing P and reached a plateau for large P. The size of micelle cores reflects the extent of intermixing of corona chains and host chains. Similar to the concept obtained from the "dry brush" and "wet brush" in polymer grafted NPs/homopolymer system, provided $P \leq N_A$, host chains readily intermix with tethered corona chains, it is so called "wet brush" case; if $P >> N_A$, host chains are largely excluded from corona chains, it is so called "dry brush" case. In "wet brush" case, PS block is stretched due to intermixing and then P2VP block shrank in order to maintain constant segmental density; this favors the formation of small micelle cores and micelles distribute throughout the host to maximize the translational entropy. On the other hand, in "dry brush" case, PS block is collapsed in order to minimize the contact with host PS due to entropic effects; this favors the formation of large micelles and micelles form close-packed structures and segregate to the free surface. Some more detailed discussion and comparison with NP/BCP/homopolymer system can be found in chapter 2.

In our work shown in chapter 2 and chapter 3, we utilized the above-mentioned PS-b-P2VP/PS blend thin films as the polymer hosts to study NP organization. The relative interactions between the NPs and the PS and P2VP-components, together with entropic interactions, generally determine the spatial organization of nanoparticles throughout the polymeric hosts. In Chapter 2, we demonstrated nanoparticle encapsulation into the micelle cores regardless of host chains P by functionalizing the surface of AuNPs with P2VP of the same chemistry as micelle cores. On average each micelle contained one or no nanoparticle. As a result of encapsulation, NP/PS-b-P2VP/PS system exhibited a higher density of

smaller micelles compared to the PS-b-P2VP/PS polymer blends. Subsequently in chapter 3, we further examined the precise control of NP locations in such polymer blend thin films. The spatial distribution of PS grafted NP in this blend thin film is characterized by a morphological diagram in terms of NP curvature, 1/R vs. the degree of polymerization of grafted chain, N. The NP distributions range from predominantly residing at external interfaces (the free surface or/and the substrate) to "decorating" micelles.

1.3.2. Diblock copolymer/star-shaped polymer blend thin films

The morphology and structure of polymer blends composed of linear chains has been intensively studied. However, the influence of the chain architecture remains unexplored particularly in thin film states. Recently, the structures and properties of polymeric molecules that possess star-shaped architectures has drawn considerable interest. This study will investigate the influence of the star-shaped polymers on the morphological behaviors of thin film blends.

Unlike a linear polymer composed of a single free chain, a star-shaped polymer contains a number of linear chains covalently tethered to a core molecule. This class of polymer exhibits unique physical properties (wetting, aging and dynamics), generally associated with topology and related entropic effects.[51,52] Star-shaped polymers are well known to exhibit stronger absorption to interfaces than their linear analogues. This is due to less conformational entropy loss for star-shaped molecules absorbing to interfaces. The magnitude of entropy loss upon adsorption is associated with the number of arms, f and the degree of polymerization of the arm, N_{arm}. In mixture with linear chains, star-shaped molecules are found to preferentially segregate towards interfaces.[25,53-55] In addition, they also tend to possess lower cohesive energy densities, leading to a lower surface energy.

In chapter 4, we are particular interested in understanding how *f* and N_{arm} of star-shaped polymers (star-shaped PS) may affect the organization of BCP chains (PS-b-P2VP) as well as the phase behaviors of BCP/star-shaped thin film mixtures. BCP chains also self-assembled into micelles in star-shaped PS as discussed in the linear PS. The system could be tailored to exhibit miscibility or phase separation of micelles in star-shaped polymer hosts and the resultant composition profiles near the surface showed variations in BCP concentration, ranging from BCP depletion to BCP excess; this cannot be achieved in their linear analog system.

These results imply that this is an especially important multi-component polymeric system for various applications since phase behaviors and morphologies, a critical factor responsible for physical properties, can be tailored even without changing chemistry of polymers. With well controlled phase behaviors, this thin film polymer blend system is anticipated as a promising PNC matrix to template NP organization.

1.4. References

(1) Atwater, H. A.; Polman, A. *Nature Materials* 2010, *9*, 205.
(2) Gangopadhyay, R.; De, A. *Chemistry of Materials* 2000, *12*, 608.
(3) Hu, G. J.; Zhao, C. G.; Zhang, S. M.; Yang, M. S.; Wang, Z. G. *Polymer* 2006, *47*, 480.
(4) Kashiwagi, T.; Grulke, E.; Hilding, J.; Groth, K.; Harris, R.; Butler, K.; Shields, J.; Kharchenko, S.; Douglas, J. *Polymer* 2004, *45*, 4227.
(5) Nath, N.; Chilkoti, A. *Analytical Chemistry* 2002, *74*, 504.
(6) Nasongkla, N.; Bey, E.; Ren, J.; Ai, H.; Khemtong, C.; Guthi, J. S.; Chin, S.-F.; Sherry, A. D.; Boothman, D. A.; Gao, J. *Nano Letters* 2006, *6*, 2427.
(7) Kumar, S. K.; Jouault, N.; Benicewicz, B.; Neely, T. *Macromolecules* 2013, *46*, 3199.
(8) Green, P. F. *Soft Matter* 2011, *7*, 7914.
(9) Xi, J. Q.; Schubert, M. F.; Kim, J. K.; Schubert, E. F.; Chen, M.; Lin, S.-Y.; Liu, W.; Smart, J. A. *Nature Photonics* 2007, *1*, 176.
(10) Jo, A.; Joo, W.; Jin, W.-H.; Nam, H.; Kim, J. K. *Nature Nanotechnology* 2009, *4*, 727.
(11) Ganesan, V.; Jayaraman, A. *Soft Matter* 2014, *10*, 13.
(12) Ferreira, P. G.; Ajdari, A.; Leibler, L. *Macromolecules* 1998, *31*, 3994.
(13) Matsen, M. W.; Gardiner, J. M. *Journal of Chemical Physics* 2001, *115*, 2794.
(14) Borukhov, I.; Leibler, L. *Macromolecules* 2002, *35*, 5171.
(15) Kim, B.; Ryu, D. Y.; Pryamitsyn, V.; Ganesan, V. *Macromolecules* 2009, *42*, 7919.
(16) Xu, J.; Qiu, F.; Zhang, H.; Yang, Y. *Journal of Polymer Science Part B-Polymer Physics* 2006, *44*, 2811.
(17) Kim, J. U.; Matsen, M. W. *Macromolecules* 2008, *41*, 4435.
(18) Pryamtisyn, V.; Ganesan, V.; Panagiotopoulos, A. Z.; Liu, H.; Kumar, S. K. *Journal of Chemical Physics* 2009, *131*.
(19) Roan, J. R.; Kawakatsu, T. *Journal of Chemical Physics* 2002, *116*, 7283.
(20) Striolo, A.; Egorov, S. A. *Journal of Chemical Physics* 2007, *126*.
(21) Lee, J. Y.; Buxton, G. A.; Balazs, A. C. *Journal of Chemical Physics* 2004, *121*, 5531.
(22) Lee, J. Y.; Shou, Z. Y.; Balazs, A. C. *Macromolecules* 2003, *36*, 7730.
(23) McGarrity, E. S.; Frischknecht, A. L.; Frink, L. J. D.; Mackay, M. E. *Physical Review Letters* 2007, *99*.
(24) McGarrity, E. S.; Frischknecht, A. L.; Mackay, M. E. *Journal of Chemical Physics* 2008, *128*.
(25) Minnikanti, V. S.; Archer, L. A. *Journal of Chemical Physics* 2005, *123*.
(26) Israelachvili, J. N. In *Intermolecular and Surface Forces (Third Edition)*; Israelachvili, J. N., Ed.; Academic Press: San Diego, 2011, p 253.
(27) Meli, L.; Arceo, A.; Green, P. F. *Soft Matter* 2009, *5*, 533.
(28) Kim, J.; Green, P. F. *Macromolecules* 2010, *43*, 1524.
(29) Chen, X. C.; Green, P. F. *Soft Matter* 2011, *7*, 1192.
(30) Bates, F. S.; Fredrickson, G. H. *Annual Review of Physical Chemistry* 1990, *41*, 525.
(31) Matsen, M. W.; Bates, F. S. *Macromolecules* 1996, *29*, 1091.
(32) Bates, F. S.; Fredrickson, G. H. *Physics Today* 1999, *52*, 32.
(33) Vaia, R. A.; Maguire, J. F. *Chemistry of Materials* 2007, *19*, 2736.
(34) Bockstaller, M. R.; Mickiewicz, R. A.; Thomas, E. L. *Advanced Materials* 2005, *17*, 1331.
(35) Haryono, A.; Binder, W. H. *Small* 2006, *2*, 600.

(36) Kim, B.; Fredrickson, G.; Hawker, C.; Kramer, E. *Langmuir* 2007, *23*, 7804.
(37) Kim, B. J.; Bang, J.; Hawker, C. J.; Kramer, E. J. *Macromolecules* 2006, *39*, 4108.
(38) Kim, B. J.; Fredrickson, G. H.; Kramer, E. J. *Macromolecules* 2008, *41*, 436.
(39) Thompson, R. B.; Ginzburg, V. V.; Matsen, M. W.; Balazs, A. C. *Science* 2001, *292*, 2469.
(40) Chiu, J. J.; Kim, B. J.; Yi, G. R.; Bang, J.; Kramer, E. J.; Pine, D. J. *Macromolecules* 2007, *40*, 3361.
(41) Kim, B. J.; Chiu, J. J.; Yi, G. R.; Pine, D. J.; Kramer, E. J. *Adv. Mater.* 2005, *17*, 2618.
(42) Lee, J. Y.; Thompson, R. B.; Jasnow, D.; Balazs, A. C. *Macromolecules* 2002, *35*, 4855.
(43) He, L. L.; Zhang, L. X.; Liang, H. J. *Journal of Physical Chemistry B* 2008, *112*, 4194.
(44) He, L. L.; Zhang, L. X.; Liang, H. J. *Journal of Polymer Science Part B-Polymer Physics* 2009, *47*, 1.
(45) Bae, J.; Kim, J.; Park, J. *Thin Solid Films* 2014, *562*, 338.
(46) Lin, Y.; Boker, A.; He, J. B.; Sill, K.; Xiang, H. Q.; Abetz, C.; Li, X. F.; Wang, J.; Emrick, T.; Long, S.; Wang, Q.; Balazs, A.; Russell, T. P. *Nature* 2005, *434*, 55.
(47) Kim, J.; Green, P. F. *Macromolecules* 2010, *43*, 10452.
(48) Leibler, L.; Orland, H.; Wheeler, J. C. *Journal of Chemical Physics* 1983, *79*, 3550.
(49) Shull, K. R. *Macromolecules* 1993, *26*, 2346.
(50) Chen, X. C.; Yang, H. X.; Green, P. F. *Macromolecules* 2011, *44*, 5758.
(51) Likos, C. N.; Lowen, H.; Watzlawek, M.; Abbas, B.; Jucknischke, O.; Allgaier, J.; Richter, D. *Physical Review Letters* 1998, *80*, 4450.
(52) Vlassopoulos, D.; Fytas, G.; Pakula, T.; Roovers, J. *Journal of Physics-Condensed Matter* 2001, *13*, R855.
(53) Minnikanti, V. S.; Archer, L. A. *Macromolecules* 2006, *39*, 7718.
(54) Qian, Z.; Minnikanti, V. S.; Sauer, B. B.; Dee, G. T.; Archer, L. A. *Macromolecules* 2008, *41*, 5007.
(55) Qian, Z. Y.; Minnikanti, V. S.; Archer, L. A. *Journal of Polymer Science Part B-Polymer Physics* 2008, *46*, 1788.

CHAPTER 2.
NANOPARTICLE ENCAPSULATION IN THIN FILM MICELLAR STRUCTURE

Zhao, J.; Chen, X. C.; Green, P. F. *Soft Matter* **2013**, *9*, 6128. - Reproduced by permission of The Royal Society of Chemistry

2.1. Introduction

Phase separated A-b-B diblock copolymers (BCP), well known to exhibit morphologies with the A and B-phases possessing varying geometrical symmetries (spheres, cylinders, lamellae and gyroids),[1] have been used as scaffolds for nanoparticles (NPs). These BCP/NP systems exhibit properties that render them viable for diverse applications that include high-efficient catalysts, chemical sensors, high-density magnetic data storage and electronic devices.[2-5] One common strategy employed to incorporate nanoparticles within BCP hosts is to *in-situ* synthesize the nanoparticles, via a reduction of metal precursors, into one of the blocks of the BCP.[6-12] However, a significant drawback of this strategy is that the size, shape and arrangements of nanoparticles into ordered BCP phases are difficult to control. A more common strategy is to synthesize, ex-*situ*, nanoparticles of specific sizes and chemistries and then form physical blends, from solution, with the BCPs.[13-16] This strategy

enables precise control of the locations of the nanoparticles through control of the size and surface chemistries of nanoparticles during synthesis. A number of scenarios regarding NP localizations are possible under such conditions. Those nanoparticles, sufficiently small in size compared to the domain dimensions, preferentially locate within the domains or in the A/B interfacial region where they would be thermodynamically compatible. The distribution of the small NPs throughout the appropriate domain provides them with translational entropy.[13,17,18] Larger nanoparticles, of an appropriate range of sizes, preferentially segregate to the center of the appropriate domain.[17] Residing primarily at the center of the domain minimizes the conformational energy of block chains. Recent investigations on systems where the NPs surfaces are grafted with short homopolymer chains at sufficiently high grafting densities reveal that the location of nanoparticles can be tailored to reside either within one host or within the A/B interfacial region.[19-22]

The nanoparticle distributions within the BCP hosts are also influenced by defects, grain boundaries in the bulk and dislocations in thin films. In the bulk, nanoparticles exhibit a tendency to segregate to high-angle tilt grain boundaries: Chevron, Omega, T-junction /twist grain boundaries.[23,24] In thin film BCPs, nanoparticles of sufficiently large- sizes that would normally be accommodated at the center of the domains, preferentially segregate to the core of edge dislocations, as recently shown by Kim et al.[25] Parenthetically, for thin BCP films, either the A or B component would exhibit an affinity for an interface; the interior morphology would be composed of alternating A or B layers, provided the asymmetry between the sizes of the A or B blocks is not too large. Surface relief structures, Islands and holes, develop at the free surface via a nucleation process, when the films are not of an optimal thickness. The islands, or holes, are accommodated by the formation of edge

dislocations. When the nanoparticles are located within an edge dislocation, the chains that comprise the dislocation undergo less stretching and therefore gain conformational entropy.

Finally, we note that for sufficiently high nanoparticle concentrations, the domains can no longer accommodate all the nanoparticles, in part because the entropic penalties associated with chain deformation are too high. Consequently the system may undergo a morphological transition.[26] For example, Yeh et al. showed evidence of a morphological transformation of polystyrene-b-poly(4-vinylpyridine) (PS-b-P4VP) system, from a hexagonal structure to lamellar structure, with confinement of CdS nanoparticles within the P4VP domains.[27] Kim et al. showed that several morphologies may coexist in a single polystyrene-b-poly(2-vinylpyridine) (PS-b-P2VP) film due to variations in the local concentration of Au nanoparticles, as a function of depth within the film.[28]

In the foregoing we briefly discussed how the nanoparticle organization is determined by the morphology of the phase separated copolymer, through competing enthalpic and various entropic interactions. In thin film homopolymers brush coated nanoparticle organization is controlled by a number of competing interactions: particle-particle interactions, translational entropy of the nanoparticles and entropy (conformational and translational) of the host chains[29]. The entropic interactions between the brush chains and the host chains, and interactions between the tethered particles and the interfaces (free surface and substrate) are characterized by the particle curvature, length of tethered chains and the length of the host chains.[30-32] These are reasonably well understood and a phase diagram can be experimentally prepared to identify regions of miscibility and non-miscibility for athermal systems.[33]

In this chapter we are particularly interested in understanding nanoparticle organization in thin film BCP /homopolymer systems. BCP chains mixed with a selective homopolymer chains, at low BCP concentrations, also exhibit a tendency to form ordered localized structures (spheres, cylinders, lamellae and vesicles).[34] For example, in an A-b-B/A blend, micelles, with inner cores of B-type chains and outer coronas of A-type chain segments, within the host of A-type chains are known to form.[35] Recently our group showed that PS-b-P2VP self-organized into spherical micelles with an inner core of P2VP and an outer corona of PS in thin film PS hosts.[36] The average diameter of micelle cores increased with increasing host chain degree of polymerization P and reached a plateau at large P. These micelles segregated at the free surface, provided the surface tension of the corona chains is lower than that of the chains that constitute the core. The preferential segregation of the micelles toward interfaces is engendered by the fact that the corona chains suffer a lower entropy cost at interfaces than the linear chain homopolymers. For large values of $P>>N_A$, where N_A is the degree of polymerization of the A-type chains, the micelles exhibit a tendency to form close packed structures. Based on the foregoing, the natural question therefore is how are the metallic nanoparticles distributed within BCP/homopolymer blend of micellar structure? We investigated this question in the following system: mixtures of P2VP-coated gold nanoparticles, PS-b-P2VP copolymer and PS homopolymer. One of the surprising findings in this study is that the morphology differs from that of the PS-b-P2VP/PS system with a very small weight fraction of nanoparticles. The micelles either encapsulate one nanoparticle, or no nanoparticles; only a small fraction of micelles contain more than one nanoparticle.

2.2. Experimental Section

The gold nanoparticles (AuNPs) onto which poly(2-vinylpyridine) (P2VP) chains were grafted were synthesized by employing a modification of the two-phase arrested precipitation methods.[37] We used the following materials in our synthesis: Gold(III) chloride hydrate ($HAuCl_4$), tetraoctylammonium bromide (TOAB), sodium borohydride ($NaBH_4$) and toluene were purchased from Sigma-Aldrich; thiol-terminated P2VP molecules were purchased from Polymer Source (M_n= 1300g mol^{-1}, M_w/M_n = 1.08). The Au (III) ions were transferred from an aqueous solution of $HAuCl_4$ to toluene in the presence of TOAB. After discarding the aqueous phase, an aqueous $NaBH_4$ solution was added, drop-wise, into the organic phase while stirring. The reaction mixture was stirred overnight after which the aqueous phase was removed. Subsequently, the thiol-terminated P2VP ligands, which were dissolved in toluene, were added to the reaction mixture; the mixture was stirred for half an hour. The synthesized AuNPs were washed at least 10 times using toluene and cyclohexane to remove excess ligands and salts in the reaction mixture. After purification, the nanoparticles were dried at room temperature and then dissolved in toluene.

The AuNPs possessed an average core diameter d=6.1$\pm$3.2 nm and a grafting density of σ= 1.9 chains per nm^2. The average diameter of the AuNPs was determined using scanning transmission electron microscopy (STEM); at least 500 nanoparticles were analyzed. Thermogravimetric analysis (TGA) measurements were performed using a TA2960 instrument, following a heating rate protocol of 10 ^oC min^{-1}, to determine the weight fractions of gold and polymer ligands. The grafting density was calculated using the following information: the weight fractions of gold NPs and polymer ligands, the average

particle size and the densities of each species. We will refer to these nanoparticles as P2VP-AuNPs in the manuscript.

The diblock copolymer polystyrene-b-poly(2-vinylpyridine) (PS-b-P2VP) was obtained from Polymer Source Inc.; the number average molecular weights of the components of copolymer were M_n(PS) = 50,900 g mol^{-1} and M_n(P2VP)=29,100 g mol^{-1} and their degrees of polymerization were N_{PS}=489 and N_{P2VP}=277 respectively. Varying molecular weights of the PS homopolymers (M=13,000 g mol^{-1} (P=125); 152,000 g mol^{-1} (P=1460); 590,000 g mol^{-1} (P=5660) and 1600,000 g mol^{-1} (P=15400) were purchased from Pressure Chemical Co. The copolymer and homopolymer solutions were mixed such that the weight ratio of PS-b-P2VP to PS was 1:4. The mixtures were shaken for at least 2 hours after which the AuNPs were added to prepare 1wt% AuNPs/polymer blend solutions. The 1wt% AuNPs/polymer solutions were shaken for at least 2 hours prior spin-coating onto silicon nitride (Si_3N_4)-coated silicon substrates (WaferNet, Inc). The films were subsequently dried in vacuum at 65 ^{o}C overnight and annealed at 160 ^{o}C for 4 hours. The thicknesses of the resulting films, after drying, were controlled to be 110 $\pm$ 5 nm, as measured using a spectroscopic ellipsometer (J.A.Woollam Co.).

Transmission electron microscopy (TEM), was performed using a JOEL 2010F in a scanning mode (STEM), equipped with a high angle annular dark field (HAADF) detector (Z-contrast), operated at an accelerating voltage of 200 kV, to characterize the micelle formation and lateral distributions of AuNPs in the films. The STEM samples were prepared by first spin casting the Au/polymer blend solutions onto glass slides; the films were then floated onto a deionized water bath. They were then transferred onto Si_3N_4 grids (SiMPore Inc.) and subject to the same processing methods described above. The films were

subsequently exposed to iodine vapor for 1 hour to selectively stain the P2VP component. The size of micelle cores and the number densities of micelles were calculated using ImageJ software. More than 200 micelles from three to four different areas of each film were analyzed in order to ensure that the information discerned from the samples was representative of the behavior for each film. We note that the micelles were fully developed within four hours of annealing. For annealing times longer than four fours the size distribution of micelles did not change, even after two days (see Appendix A). This provides us with confidence that our results represent a realistic and true behavior of the system.

The depth profiles of copolymer and Au in the films were obtained using secondary ion mass spectroscopy (SIMS). These measurements were performed using a Physical Electronics 6650 Quadrupole instrument by Dr. Tom Mates, University of California, Santa Barbara. The combination of STEM and SIMS enabled the determination of spatial distributions of micelles and nanoparticles in the films.

2.3. Results and Discussion

We know from our prior study of the PS-b-P2VP/ PS thin film mixtures that the PS-b-P2VP copolymer chains aggregate to form micelles, processing an inner core of the P2VP block and an outer corona of the PS component. Additionally, copolymer chains adsorb onto the substrate, forming a brush layer; the P2VP component exhibits a preferential affinity for the more polar substrate. Only a negligible fraction of the remaining copolymer chains remain free within the PS host.[36] In the STEM images in Figure 2 - 1, the P2VP regions, stained by iodine vapor, are bright and the AuNPs appear as white spots. It is observed that, regardless of the PS host degree of polymerization P, AuNPs appear on the bright domains, indicating that the nanoparticles are preferentially located within the

spherical micelle cores. In contrast, if AuNPs are not located in the micellar cores, statistically, they would be seen everywhere in the film rather than only on the bright domains. Since P2VP and PS are thermodynamically incompatible, characterized by positive Flory-Huggins parameter χ=0.11, the P2VP-AuNPs gain enthalpic energy when they are encapsulated within the P2VP micelle cores. This point will be revisited below, when we discuss the morphology of the nanoparticle mixtures.

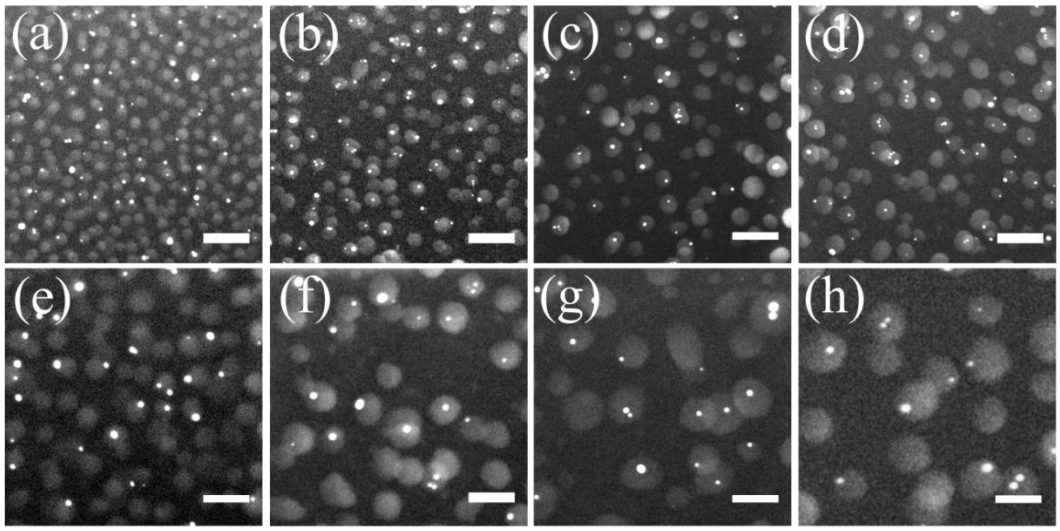

Figure 2 - 1. Scanning transmission electron micrographs (STEM) of AuNPs in thin film PS-b-P2VP/PS mixtures (weight ratio of 1:4) with different host PS degrees of polymerization: (a,e) P=125, (b,*f*) P=1460, (c,g) P=5660 and (d,h) P=15400. All films were approximately 110nm thick. The P2VP cores stained with iodine vapor appear as bright domains and AuNPs appear as white spots. The scale bar represents a distance of 100nm in (a-d) and it represents 50nm in (e-h). The relative contrast of the objects in the images is representative of its location in relation to the free surface.

Having shown that the nanoparticles are sequestered within in the micelles, the micelle diameter, D_{core}, and the number density of micelles, $n_{micelle}$, in the AuNP/PS-*b*-P2VP/PS and the PS-*b*-P2VP/PS thin film blends are now compared. The data in Figure 2 - 1 and Figure 2 - 2, reveal that the average diameters of micelle cores, $D_{core,}$ in both systems,

increase with increasing P, reaching a plateau when $P \geq 5660$. That D_{core} is largest for $P >> N_{PS}$ is to be expected. Under conditions for $P \gg N_{PS}$, the long host chain would be largely excluded from the micellar coronas. As discussed earlier, this so-called "dry brush" condition ($P >> N_{PS}$) favors the formation of large close packed micelles, which minimizes the corona/host chain interactions. When $P \sim N_{PS}$, the short host chains readily intermix with the micelle coronas in order to gain the translational entropy. As a result of intermixing, the PS coronas are stretched and the P2VP cores are concurrently compressed in order to maintain a constant segmental density. This so-called "wet brush" condition favors the formation of smaller micelles, because it maximizes the extent of intermixing between the host and corona chains. The average diameters of the micelles in the nanoparticle mixtures are smaller than those in the pure blend for high molecular weight PS host ($P > N_{PS}$) as shown in Figure 2 - 2a

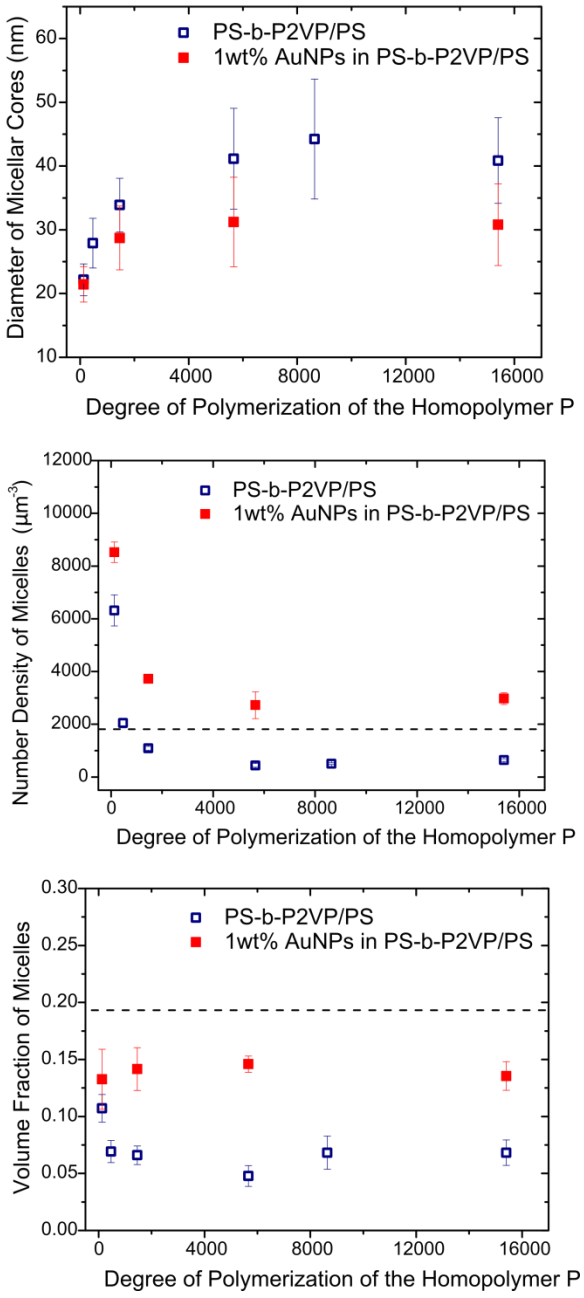

Figure 2 - 2. Plotted as a function of degree of polymerization, P, of the PS host are (a) the average diameter of micelle cores, Dcore, (b) number density of micelles, nmicelle and (c) volume fraction of micelles, vmicelle. The dashed line in part (b) represents t the number density of AuNPs, N_{AuNP}. The dashed line in part (c) represents the volume fraction of PS-b-P2VP. Open navy square represents thin film PS-b-P2VP/PS mixtures retrieved from ref.36. Solid red square represents 1wt% AuNPs in PS-b-P2VP/PS thin film mixtures.

The increase of D_{core} with increasing P is accompanied by decreases in the number densities of micelles $n_{micelle}$ with increasing P, for both systems. With regard to the nanoparticle blends, the data in Figure 2 - 2 show that for the largest values of P= 15400, $n_{micelle}$ = 2940 μm^{-3} and for P=125, $n_{micelle}$= 8520 μm^{-3}. The values of $n_{micelle}$ were determined by counting the number of micelles per unit area in the STEM images; these values were reconciled with the film thickness. The data in Figure 2 - 2 also reveal that the densities of micelles in the NP/PS-b-P2VP/PS blend, $n_{micelle}$, are larger than those of the pure blends, for all PS homopolymer chain lengths. In the pure blend, the increase of $n_{micelle}$ is primarily reconciled by the fact that the average diameter D_{core} of the chains decreases with increasing P. This is accommodated by a redistribution of copolymer chains among the micelles; some of the copolymer chains migrate to the substrate to increase the size of the brush layer. The brush layer thickness reaches its maximum value when $P>>N_{PS}$, as discussed in our previous publication. Note that since the fraction of free copolymer chains scales as $\exp(-\chi N)$ the fraction of free copolymer chains in the PS host is extremely low: $N=N_{PS}+N_{P2VP}$ =489+277=766 and Flory-the Huggins parameter χ=0.11[1], so χN=8.47.

While the dependencies of D_{core} and $n_{micelle}$ on P, in Figure 2 - 2a and Figure 2 - 2b, appear to be consistent, the P-dependencies of the volume fraction of the micelles, $v_{micelle}$, in the NP blend is surprising (see Figure 2 - 2c). In contrast to the pure system, $v_{micelle}$ remains relatively independent of P, within experimental error, though one could argue that it increased slightly with increasing P. The essential point, nevertheless, is that the behavior is fundamentally different from that of the pure blend. We now explain how $v_{micelle}$ was calculated. The volume fraction of the micelle cores $v_{core} = \pi (D_{core})^3 n_{micelle}/6$ and $v_{micelle}= v_{core}/f_{P2VP}$, where f_{P2VP} is the volume fraction of P2VP component in PS-b-P2VP ($f_{P2VP}=M_{P2VP}\rho_{PS}/(M_{PS}\rho_{P2VP}+M_{P2VP}\rho_{PS})$, where M_{P2VP}=29,100 g mol^{-1}, M_{PS}=50,900 g mol^{-1} and

the densities of PS and P2VP component are ρ_{PS}=1.045 g cm^{-3} and ρ_{P2VP}=1.18 g cm^{-3}). The calculation of $v_{micelle}$ does not include the penetration of host chains into the coronas.

The primary points that follow from the foregoing are: (1) the number density of micelles in the nanoparticle blend is larger than that of the pure system; (2) the average diameters of the micelles in the NP mixtures are smaller for high molecular weight PS host ($P>N_{PS}$); (3) the number of BCP chains that contribute to micelle formation in the NP-BCP mixture is much larger than in the pure system. We now examine further details of the organization of the micelles and the nanoparticles within the films by SIMS (Figure 2 - 3). SIMS was used to measure the depth profiles of the components of the copolymer chains and Au within the films. The signal from CN group, originating from the P2VP block, will be used to identify the location of the micelles, as a function of depth within the films. The primary contribution to the CN signal is from the P2VP block of the BCP chains; the contribution from P2VP chains grafted onto AuNP surfaces is negligible (~3%). In each sample, the largest peaks are located at the substrate and at the free surface. Based on the use of standards, the peaks at the substrate represent layers that range in thickness from $h_{(AuNPs/BCP/PS)}$=17.3 nm for P=125 to $h_{(AuNPs/BCP/PS)}$=28.5 nm when P=15,400. These layers are thicker than the brush layers that formed in the pure PS-b-P2VP/PS system, where $h_{(BCP/PS)}$=10.8 nm for P=125 and $h_{(BCP/PS)}$=19 nm for P=15400. Note that the thickest brush layer that would be expected to form at the substrate would be one half the lamellar thickness, $h_{max}=L/2$. In the strong segregation limit ($\chi N \gg 1$), $L=aN^{2/3}\chi^{1/6}$ =40 nm where the statistical segmental length a=0.69nm; degree of polymerization of copolymer $N=N_{PS}+N_{P2VP}$ =489+277=766 and Flory-Huggins parameter χ=0.11[1]. Therefore, the thickness of brush layer should be L/2=20 nm when $P \gg N_{PS}$.

One might surmise that because $h_{(AuNPs/BCP/PS)}>h_{max}$, the earlier observation (Figure 2 - 2c) that a larger fraction of copolymer chains comprise the micelles in the NP blends would not be consistent. The observation suggests that the layer at the substrate would be thinner than $h_{(BCP/PS)}$. Insight into the reason behind this apparent discrepancy ($h_{(AuNPs/BCP/PS)}>h_{max}$) becomes evident from close examination of the profiles in Figure 2 - 3. The location of the Au peak in relation to the P2VP peaks near the substrate is consistent with micelles containing AuNPs, organized in close proximity to the brush layer. We know from our prior research in the PS-b-P2VP/PS system that the micelles segregate and organize at the free surface and the brush layer forms at the substrate, when $P>>N_{PS}$. The breadths of the P2VP peaks in the SIMS profiles are consistent with contributions from two layers, a brush layer and a layer of micelles containing nanoparticles; this is especially apparent in Figure 2 - 3d. Please note that the brush layer cannot accommodate nanoparticles due to large free energy cost associated with introducing large inclusions, as predicted by Kim and O'Shauhnessy.[38] They extended self-consistent mean field theory to calculate the critical diameter of inclusions b_{max}, $b_{max}\sim N^{1/4}$, where N is the degree of polymerization of polymer brush. Nanoparticles larger than b_{max} are expelled from polymer brush. For our systems this prediction indicates that $b_{max}=5.3$ nm using $N=N_{PS}+N_{P2VP}=766$ ($b_{max}<d=6.1$ nm, average diameter of AuNPs), suggesting that large AuNPs would not be accommodated by the brush layer. Consequently, the AuNPs near the substrate are encapsulated in the P2VP cores of micelles adjacent to the brush layer.

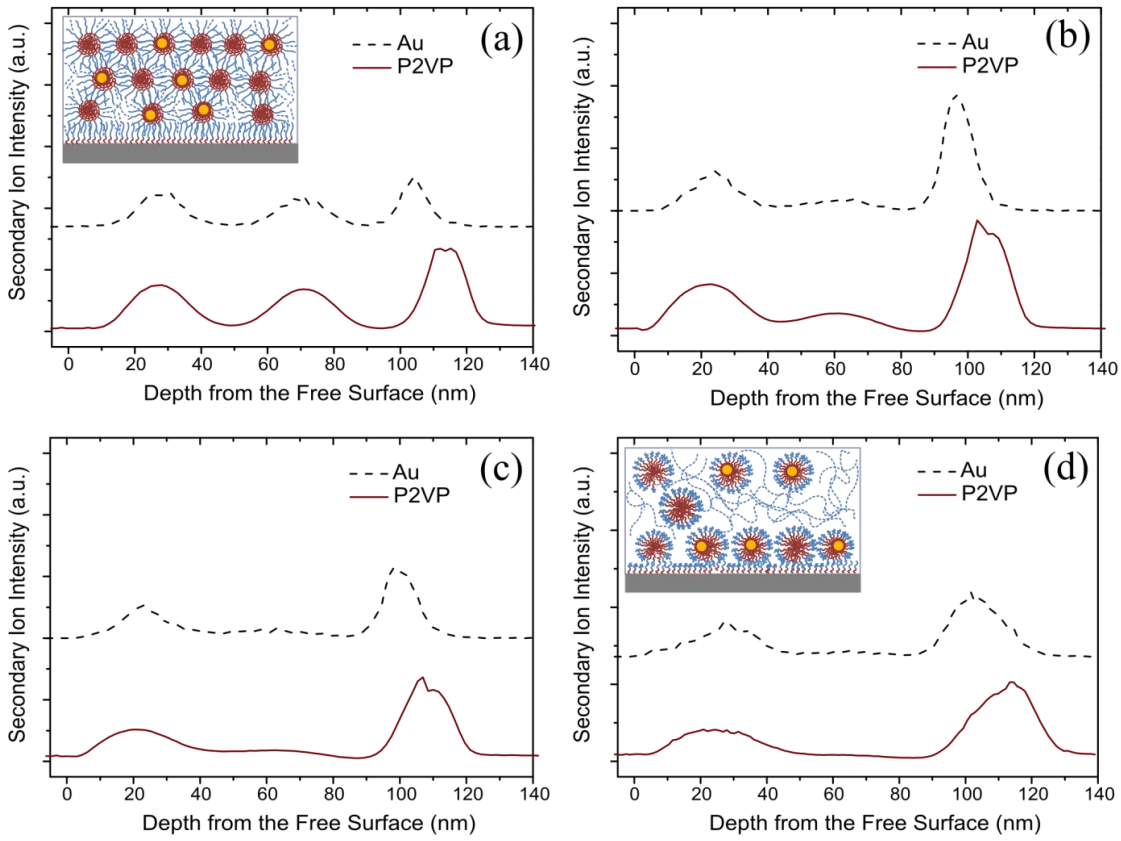

Figure 2 - 3. Depth profiles of AuNPs and of the P2VP components in a series of blends, each of average thickness 110 nm: (a) P=125, (b) P=1460, (c) P=5660 and (d) P=15400. The insets in parts (a) and (d) represent schematics of corresponding film morphologies (micelle organization and the brush layer).

The discussion regarding the morphology of the films is now continued. The outer surface peaks of the SIMS profiles indicate that micelles reside at the surface of each sample. The profile in Figure 2 - 3a, with three peaks, shows evidence of three layers of micelles, and the brush layer. When P increases, the micelles exhibit a tendency to segregate to the interfaces; this leads to a reduction of the concentration of micelles in the center of the films. The profile in Figure 2 - 3d is most illustrative of this point; two peaks exist. The first represents the surface layer of micelles and the second represents one layer of micelles and

the brush layer. The interfacial segregation of micelles is expected because the host chains are excluded from the corona when $P>>N_{PS}$. Under these conditions, the micelle-micelle interactions are such that the long host chains exhibit a tendency to migrate from between the micelles in order to avoid a loss of conformational entropy, due to confinement. Note that when PS host chains are shorter $P\sim N_{PS}$ or $P<N_{PS}$, the micelle coronas intermix with short PS host chains, leading to an entropic gain of the homopolymer chains. Because of the corona/host chain mixing, the PS corona chains become stretched and the micelle cores are compressed in order to maintain a constant segmental density. This leads to increased $n_{micelle}$ and decreased D_{core}. In summary, for short host chains, the micelles gain translational entropy by distributing throughout the film and the host chains gain translational entropy by mixing with the micelle corona chains. When $P>>N_{PS}$, the micelles increase in size and segregate at the interfaces to minimize the micelle/homopolymer chain interactions ("dry" brush condition). These arguments regarding the change in $n_{micelle}$, D_{core} and the spatial organization of the micelles apply equally to pure blends and the nanoparticle blends.

In the absence of a theoretical framework that would predict the distribution of brush coated nanoparticles in thin film NP/BCP/homopolymer systems, we make a number of qualitative observations, supported by experimental data. These observations should provide meaningful insight that would motivate future theory and simulations. We begin by noting that the P2VP-Au nanoparticles would be phase segregated within the PS host due to the incompatibility between the P2VP and PS chains. We note, further, that low molecular weight (N=10) PS-coated Au nanoparticles, of the similar core diameter used in this study, would be phase segregated; they reside at the interfaces (free surface and substrate) of the PS films, as shown by experiments in our laboratory. [33] In the case of the BCP/PS mixtures, all the P2VP-Au NPs are encapsulated within the micelles cores due to the incompatibility

between P2VP brush chains and PS host chains (coronas and host chains). On average, as shown in Figure 2 - 4e, one nanoparticle is encapsulated per micelle, due to the strong P2VP/Au interaction. [39,40] So this dispersion of AuNPs maximizes the interfacial area of interaction between NPs surface and P2VP chains, leading to a maximum gain in enthalpic energy.

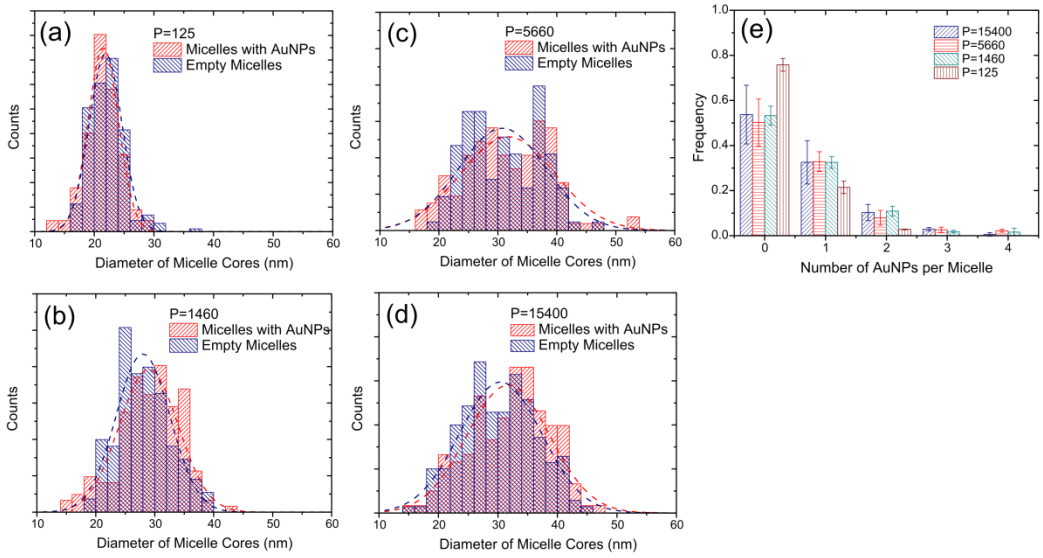

Figure 2 - 4. Histograms of diameter of micelle cores with and without AuNPs in a series of AuNPs/polymer blends (a) P=125, (b) P=1460, (c) P=5660 and (d) P=15400. The size distributions of both empty micelles and micelles with nanoparticles are fitted to Gaussian profile (dash line). (e) the distributions of AuNPs within micelle cores, as determined from the STEM measurements

The plot in Figure 2 - 2a indicates that the micellar size of the AuNPs/BCP/PS(P=125) sample remains similar to that of the neat BCP/PS(P=125) samples. On the other hand for the higher molecular weight PS hosts, specifically in the case of $P>>N_{PS}$ (dry brush conditions), the micelle size of AuNP/BCP/PS system is much smaller than that of the neat BCP/PS sample; This is associated with an appreciable increase

of number density of micelles, $n_{micelle}$ in the AuNP/BCP/PS system. It is noteworthy that for the lowest molecular weight host, P=125, $n_{micelle}$ is much greater than the number density of nanoparticles, N_{AuNP} (The N_{AuNP} is determined by counting the number of nanoparticles per unit area in the STEM images over the film thickness). However, for the "dry-brush" systems ($P>>N_{PS}$), $n_{micelle}<N_{AuNP}$ (see Figure 2 - 2b). The system, in an effort to maximize the enthalpic interactions between the P2VP tethered AuNPs and the inner micelle P2VP core, increases the number of micelles in order to encapsulate all nanoparticles. A large fraction of micelles contain no nanoparticles. We speculate that the existence of a number of empty micelles would be to maximize the translational entropy of nanoparticles while minimizing the enthalpic interactions. The larger $n_{micelle}$ in the nanocomposite (AuNPs/BCP/PS) is also contributed by a larger fraction of copolymer chains participating in micelle formation in the nanocomposite than in the neat BCP/PS system. This is evident from the fact that the average brush layer is thinner in the NP samples than in the pure system. The density of chains in the brush layer is such that the nanoparticles do not intermix with the P2VP layers.

In the AuNP/BCP/PS system, the distribution of the sizes of the micelles containing nanoparticles is similar as empty micelles (see Figure 2 - 4a - d). A larger distribution of sizes would not be expected for the micelles containing nanoparticles because, on average, each micelle contains one nanoparticle and the volume of a nanoparticle is less than 1% of that of a micelle.

2.4. Concluding Remarks

The incorporation of brush coated nanoparticles in pure block copolymer hosts is well understood. Moreover, a great deal is understood about the structure of thin film

homopolymer/brush coated nanoparticle systems. The more complex system involving nanocomposites of NP/BCP/homopolymer mixtures is less well understood and such systems are of practical implications. Here we show a AuNPs/BCP/homopolymer system in which the copolymers form micelles with an inner core of P2VP block and an outer corona of PS block and a brush layer at the substrate due to the affinity of the P2VP block to the polar substrate, within the homopolymer host. The average diameter, D_{core}, of the micelles increased with increasing PS chain molecular weight, P, and the number density of micelles $n_{micelle}$ decreases with increasing PS degree of polymerization, P. This behavior is associated with a transition from a "wet brush" situation to the "dry brush" situation where the host chains are excluded from the coronas of the micelles. Under these conditions, the micelles segregate to the interfaces to minimize the host chain/corona chain interactions. The long host chains migrate from between the micelles to avoid a loss of conformational entropy. This phenomenon is well understood, as discussed in our prior study. [36]

The findings in this study suggest that the distribution of nanoparticles is dictated by the attempt of the system to minimize the enthalpic energy cost (by maximizing the interaction area between the P2VP brush coated AuNPs and the P2VP block component) and maximize the translational entropy of the nanoparticles by encapsulating one P2VP coated AuNP per micelle. In the nanocomposite the number of micelles is larger than that of the neat BCP/homopolymer system; this would be to accomplish energy minimization. The larger number of micelles enables an increase in the translational entropy of copolymer chains and of the nanoparticles. The brush coated nanoparticles do not segregate to the interfaces for the following reasons. P2VP has a higher surface energy than PS, so the NPs would not segregate to the free surface. Moreover, the P2VP segments of the copolymers form a brush layer at the substrate, thereby excluding the nanoparticles.

We have presented a strategy that would be useful to build templates in order to control the distribution of nanoparticles within a host. As such this procedure increases the "tool box" available for the synthesis/fabrication of functional materials.

2.5. References

(1) Bates, F. S.; Fredrickson, G. H. *Annu. Rev. Phys. Chem.* 1990, *41*, 525.
(2) Cheng, J. Y.; Ross, C. A.; Chan, V. Z. H.; Thomas, E. L.; Lammertink, R. G. H.; Vancso, G. J. *Adv. Mater.* 2001, *13*, 1174.
(3) Jaramillo, T. F.; Baeck, S. H.; Cuenya, B. R.; McFarland, E. W. *J. Am. Chem. Soc.* 2003, *125*, 7148.
(4) Mui, S. C.; Trapa, P. E.; Huang, B.; Soo, P. P.; Lozow, M. I.; Wang, T. C.; Cohen, R. E.; Mansour, A. N.; Mukerjee, S.; Mayes, A. M.; Sadoway, D. R. *J. Electrochem. Soc.* 2002, *149*, A1610.
(5) Warren, S. C.; Messina, L. C.; Slaughter, L. S.; Kamperman, M.; Zhou, Q.; Gruner, S. M.; DiSalvo, F. J.; Wiesner, U. *Science* 2008, *320*, 1748.
(6) Hashimoto, T.; Harada, M.; Sakamoto, N. *Macromolecules* 1999, *32*, 6867.
(7) Mayer, A. B. R.; Mark, J. E. *Colloid Polym. Sci.* 1997, *275*, 333.
(8) Mendoza, C.; Pietsch, T.; Gutmann, J. S.; Jehnichen, D.; Gindy, N.; Fahmi, A. *Macromolecules* 2009, *42*, 1203.
(9) Mossmer, S.; Spatz, J. P.; Moller, M.; Aberle, T.; Schmidt, J.; Burchard, W. *Macromolecules* 2000, *33*, 4791.
(10) Shen, H. W.; Zhang, L. F.; Eisenberg, A. *J. Am. Chem. Soc.* 1999, *121*, 2728.
(11) Sohn, B. H.; Seo, B. H. *Chem. Mater.* 2001, *13*, 1752.
(12) Sohn, B. H.; Seo, B. W.; Yoo, S. I. *J. Mater. Chem.* 2002, *12*, 1730.
(13) Chiu, J. J.; Kim, B. J.; Yi, G. R.; Bang, J.; Kramer, E. J.; Pine, D. J. *Macromolecules* 2007, *40*, 3361.
(14) Li, W. K.; Liu, S. Q.; Deng, R. H.; Zhu, J. T. *Angew. Chem. Int. Ed.* 2011, *50*, 5865.
(15) Mai, Y. Y.; Eisenberg, A. *Macromolecules* 2011, *44*, 3179.
(16) Meli, L.; Li, Y.; Lim, K. T.; Johnston, K. P.; Green, P. F. *Macromolecules* 2007, *40*, 6713.
(17) Bockstaller, M. R.; Lapetnikov, Y.; Margel, S.; Thomas, E. L. *J. Am. Chem. Soc.* 2003, *125*, 5276.
(18) Thompson, R. B.; Ginzburg, V. V.; Matsen, M. W.; Balazs, A. C. *Science* 2001, *292*, 2469.
(19) Chiu, J. J.; Kim, B. J.; Kramer, E. J.; Pine, D. J. *J. Am. Chem. Soc.* 2005, *127*, 5036.
(20) Jang, S. G.; Kramer, E. J.; Hawker, C. J. *J. Am. Chem. Soc.* 2011, *133*, 16986.
(21) Schultz, A. J.; Hall, C. K.; Genzer, J. *Macromolecules* 2005, *38*, 3007.
(22) Wang, Q.; Nealey, P. F.; de Pablo, J. J. *J. Chem. Phys.* 2003, *118*, 11278.
(23) Gido, S. P.; Thomas, E. L. *Macromolecules* 1994, *27*, 6137.
(24) Listak, J.; Bockstaller, M. R. *Macromolecules* 2006, *39*, 5820.
(25) Kim, J.; Green, P. F. *Macromolecules* 2010, *43*, 10452.
(26) Lee, J. Y.; Thompson, R. B.; Jasnow, D.; Balazs, A. C. *Macromolecules* 2002, *35*, 4855.
(27) Yeh, S. W.; Wei, K. H.; Sun, Y. S.; Jeng, U. S.; Liang, K. S. *Macromolecules* 2005, *38*, 6559.
(28) Kim, B. J.; Chiu, J. J.; Yi, G. R.; Pine, D. J.; Kramer, E. J. *Adv. Mater.* 2005, *17*, 2618.
(29) Green, P. F. *Soft Matter* 2011, *7*, 7914.
(30) Meli, L.; Arceo, A.; Green, P. F. *Soft Matter* 2009, *5*, 533.
(31) Trombly, D. M.; Ganesan, V. *J. Chem. Phys.* 2010, *133*.
(32) Kalb, J.; Dukes, D.; Kumar, S. K.; Hoy, R. S.; Grest, G. S. *Soft Matter* 2011, *7*, 1418.

(33) Kim, J.; Green, P. F. *Macromolecules* 2010, *43*, 1524.
(34) Ruzette, A. V.; Leibler, L. *Nat. Mater.* 2005, *4*, 19.
(35) Shull, K. R. *Macromolecules* 1993, *26*, 2346.
(36) Chen, X. C.; Yang, H. X.; Green, P. F. *Macromolecules* 2011, *44*, 5758.
(37) Brust, M.; Walker, M.; Bethell, D.; Schiffrin, D. J.; Whyman, R. *J. Chem. Soc., Chem. Commun.* 1994, 801.
(38) Kim, J. U.; O'Shaughnessy, B. *Macromolecules* 2006, *39*, 413.
(39) Kim, B. J.; Bang, J.; Hawker, C. J.; Kramer, E. J. *Macromolecules* 2006, *39*, 4108.
(40) Kim, B. J.; Fredrickson, G. H.; Kramer, E. J. *Macromolecules* 2008, *41*, 436.

CHAPTER 3.
SPATIAL ORGANIZATION OF NANOPARTICLES IN THIN FILM BLOCK COPOLYMER/HOMOPOLYMER HOSTS

3.1. Introduction

Polymer nanocomposites (PNCs) constitute a special class of materials with properties that include mechanical, optical, magnetic or electronic, which may be tailored through control of the nano- and meso-scale spatial distribution of nanoparticles (NPs) within a homopolymer host.[1-3] One effective strategy to control the organization of NPs within a polymer host is to graft molecules onto the surfaces of nanoparticles before incorporation into the polymer host. The NP organization throughout the homopolymer host is dictated by a complex interplay of enthalpic and entropic interactions between the grafted layer and the homopolymer host chains. The organization may be controlled by exploiting changes of the chemistries of the grafted chains and the homopolymer, the degrees of polymerization of grafted chains N, and of the polymer host, P, the surface grafting densities Σ and the nanoparticle sizes and shapes.[2,4-15]

Another interesting class of materials with specific morphologies is created by exploiting the fact that since diblock copolymers (BCPs) exhibit various morphologies (cubic, hexagonal, lamellar, bicontinuous),[16] they may be used as scaffolds for nanoparticle self-assembly.[17-21] Provided that the brush–coated NPs are sufficiently smaller than the domain dimensions, the NPs would reside within the domains with which they are thermodynamically compatible. Defects that include dislocations, in thin films, and grain boundaries in bulk materials, are also known to play an important role toward the spatial organization of larger nanoparticles within copolymer hosts.[18,22]

Of particular interest in this work is to understand the factors that control the spatial distribution of nanoparticles in mixtures of thin film A-b-B diblock copolymers (BCPs) with homopolymer hosts A, where the BCPs form micelles, with inner cores of the B-block chains and outer coronae of A-block chains.[23-25] From a technological perspective, micelles may be employed for applications that include nanoparticle encapsulation for drug delivery and antibacterial applications.[26-28] For these practical situations, it would be important to understand the role of competing enthalpic and entropic interactions on the nanoparticle organization within micellar systems. Recently we demonstrated that P2VP grafted gold nanoparticles (P2VP-Au), at low concentrations, would be sequestered within the P2VP cores of PS-b-P2VP micelles in PS hosts.[29] Each micelle contained one or no nanoparticles on average. The maximization of the nanoparticle/micelle core (i.e.: gold/P2VP) interactions, and maximization of the translational entropies of the nanoparticles and the micelles, would be responsible for the NP encapsulation.

General questions regarding the organization of nanoparticles within these complex BCP/homopolymer micellar systems remain unanswered. We designed and created systems in which PS-coated gold nanoparticles (PS-Au) were mixed with thin film

BCP/homopolymer, specifically PS-b-P2VP/PS, hosts. Micelles composed of P2VP cores and PS coronae resided with the PS hosts. The morphological behavior of this system, a plot of the radius curvature of nanoparticles, $1/R_C$, versus the degree of polymerization N of the grafted PS chains, is quantified by five different regimes. The regimes are characterized by different NP distributions, each dictated by different dominant intermolecular interactions. A key finding in this work includes specific conditions under which the NPs surround or "decorate" micelles, residing on the surface of micelles. The phase behavior of this system is necessarily more complex than the nanoparticle/homopolymer thin film systems previously studied;[6,9,11] it provides additional insight into the relative contributions of the diverse intermolecular interactions that characterize the local spatial distributions of the nanoparticles.

3.2. Experimental Section

Thiol terminated polystyrene (PS-SH) grafted gold nanoparticles were synthesized by employing a modification of the two-phase arrested precipitation methods.[30] PS-SH molecules with a series of molecular weights were purchased from Polymer Source Inc. The PS-SH nanoparticles were washed at least 10 times using toluene and methanol or ethanol to remove excess ligands in the reaction solution. After purification, the nanoparticles were completely dried at room temperature and then dissolved in toluene. The average diameters of nanoparticles were determined by scanning transmission electron microscopy (STEM). To determine this information nanoparticles solutions were drop-cast onto a 75-mesh carbon coated copper grid (Ted Pella Inc.), dried in air and examined by a JOEL 2010F TEM in a scanning mode (STEM), equipped with a high angle annular dark field (HAADF) detector (Z-contrast), operated at an accelerating voltage of 200 kV. More than 200

nanoparticles were analyzed to estimate the average size of nanoparticles. Thermo gravimetric analysis (TGA) was used to determine the weight fraction of gold and PS-SH ligands. This measurement was performed using a TA Q500 instrument and the experiments were performed at a heat rate of 10 °C/min. The grafting densities were calculated using the following information: the weight fractions of the PS-SH ligands and gold, the average size of the nanoparticles and the densities of each species. We will refer these gold nanoparticles as PS(N)-Au(d) in the manuscript. Here, d represents the average diameter of nanoparticle cores, while N represents the degree of polymerization of grafted PS-SH chains. The physical characteristics of these gold nanoparticles are listed in Table 3 - 1.

Table 3 - 1. The characteristics of gold nanoparticles coated by PS with a series of molecular weights

Nanoparticles	**[1] M_n (g/mol)**	**[2]d (nm)**	**[3]Σ (chains/nm^2)**
Au2PS10	1100	2.08 ± 0.50	1.9
Au3PS10	1100	3.03 ± 0.59	2.7
Au4PS10	1100	3.57 ± 0.57	1.5
Au6PS10	1100	5.60 ± 1.78	2.0
Au2PS29	3000	2.12 ± 0.49	1.9
Au3PS29	3000	3.11 ± 0.68	1.6
Au7PS29	3000	6.91 ± 1.9	2.1
Au4PS60	6500	3.95 ± 1.32	1.1
Au4PS280	29000	4.06 ± 1.22	1.6
Au6PS280	29000	6.34 ± 1.57	2.2
Au6PS481	50000	5.9 ± 1.02	1.2

[1] M_n = number average molecular weight of PS-SH. [2] d = the average diameter of an Au nanoparticle core, determined from the STEM images.[3] Σ= grating density of ligands.

The diblock copolymer polystyrene-b-poly(2-vinylpyridine) (PS-b-P2VP, M_n(PS) = 50,900 g/mol, degree of polymerization of PS block N_{PS} =489 and M_n(P2VP)=29,100 g/mol, degree of polymerization of P2VP block N_{P2VP}=277, polymer Source Inc) and the homopolymer polystyrene (PS, M_n =65,000 g/mol, degree of polymerization of host P=6250, Pressure Chemical Co.) were dissolved in toluene separately and mixed such that the weight ratio of PS-b-P2VP to PS was 1:4. To prepare nanocomposite samples, 0.05 weight fractions of PS coated nanoparticles were added to the polymer blend; the nanoparticles/polymer blend solutions were then shaken for at least 2 hours and immediately spin-cast onto silicon nitride (Si_3N_4) coated silicon substrates (Wafernet Inc). These samples were annealed in a vacuum oven at 65°C overnight to remove residual solvent and then annealed in a supercritical CO_2 ($scCO_2$) cell at a temperature of 50 °C and a pressure of 13.8 MPa for 24 hours. Additional details of $scCO_2$ annealing procedure are described elsewhere.[31] $ScCO_2$ is a poor solvent for both PS and PS-b-P2VP;[32] it mildly plasticizes the films enabling them to reach an equilibrium state. We note here that the solvent quality is readily controlled through changes in the temperature and $scCO_2$ pressure. The primary advantage of $scCO_2$ is its ability to plasticize samples at relatively low temperatures, thus maintaining stability of grafted PS ligands on nanoparticles. The final film thicknesses were approximately 90-100nm, measured by spectroscopic ellipsometry (J.A. Woollam Co).

The surface topography of each sample was examined, in the tapping mode, with atomic force microscopy (AFM, MFP-3D, Asylum Research) using Si cantilevers (42N/m spring constant and 320kHz intrinsic frequency, NanoWorld). The surface roughness and the power spectrum density (PSD) profile of each topographical image were extracted using the WSxM software.[33] The PSD profile provides information about the characteristic length

scales of the surface fluctuations of samples that underwent phase separation. The depth profiles of copolymer and gold in the films were obtained using dynamic secondary ion mass spectroscopy (DSIMS). These measurements were performed using a Physical Electronics 6650 Quadrupole instrument by Dr. Tom Mates, University of California, Santa Barbara.

The STEM samples were prepared by first spin coating nanoparticles/polymer blend solutions onto glass slides; the films that formed after drying were then floated onto a deionized water bath. These films were then transferred onto Si_3N_4 grids (SiMPore Inc.) and subject to the same processing methods described above. The films were subsequently exposed to iodine vapor for 1 hour to selectively stain the P2VP component. The combination of these characterization techniques, STEM, DSIMS and AFM, enabled us to determine the spatial distributions of micelles and nanoparticles within the samples.

3.3. Results and Discussion

The spatial distribution of nanoparticles within thin supported homopolymer films was discussed in earlier studies.[2,4-6,9,11-14,34,35] Thermodynamic interactions that determine the structure of these systems are now discussed in order to provide a context for understanding the more complex PS/PS-*b*-P2VP/NP thin film system. Our discussion will be restricted to the case where the grafted chains are of identical chemistry to the homopolymer host chains and the grafting densities Σ of the nanoparticles is sufficiently high that interactions between the nanoparticle cores are not relevant. Entropic interactions generally determine the spatial distribution of the nanoparticles within a polymer host when the grafted chains are of identical chemistry to the host chains. While the translational entropy promotes dispersion of the nanoparticles throughout the polymer host, interactions between the grafted brush layer and the polymer host chains may have a counterbalancing effect, under certain

conditions. The magnitudes of Σ, P and N (e.g.: N<<P) could be such that brush/host chain intermixing is extremely limited. Under these conditions the nanoparticles exhibit a tendency to aggregate and form separate phases; this minimizes the area of contact and therefore the finite interfacial tension between the host and brush layers, as well as depletion interactions. The driving force for phase separation increases with increasing nanoparticle core size, R_c. In thin films, the NPs exhibit a tendency to preferentially segregate to the external interfaces, free surface and substrate. Segregation of the NPs to interfaces is favored because the free chains gain entropy. The entropic losses experienced by the tethered chains at interfaces are lower than free chains of the same length; this provides a driving force for interfacial segregation. Moreover, the segregation of the nanoparticles to the substrates is also driven by van der Waals forces, which increases with decreasing grafted chain degree of polymerization, N. Finally, we note that dispersion of nanoparticles is generally achievable for sufficiently long chains and smaller Σ, due to enhanced brush layer/host chain intermixing. The transition from significant brush layer/host chain intermixing to limited mixing occurs when $\Sigma N^{1/2} > (P/N)^{-2}$, provided P/N < 1, and is$\Sigma N^{1/2} = 1$ if P/N >1.

Having discussed factors that determine the PS(N)-Au(d) nanoparticle distribution within thin supported homopolymer films, we are now in a position to understand the spatial distribution of these nanoparticles in thin film PS/PS-b-P2VP/NP blends. A discussion of the morphological structures of PS/PS-b-P2VP and PS/PS-b-P2VP/nanoparticle thin film blends now follows. The morphological phase diagram of $1/R_c$ versus N is subsequently developed. The remainder of the manuscript provides an explanation of the intermolecular interactions that determine the existence of the five different morphological regimes within this phase diagram.

3.3.1. Structure of PS/PS-b-P2VP and PS/PS-b-P2VP/nanoparticle thin film blends

In the case of supported PS-b-P2VP/PS thin film mixtures, the PS-b-P2VP copolymers form spherical micelles, with inner P2VP cores and outer PS coronae, within the homopolymer PS host. Secondly, the PS-b-P2VP chains form a brush layer on the substrate, due to the affinity of the P2VP block for the polar Si_3N_4 substrate.[23] The STEM image in Figure 3 - 1a shows spherical micelles in PS (P=6250) hosts. The P2VP cores, of average diameter 28 nm and number density of micelles 3600 μm^{-3}, appear bright in the images due to staining of the sample by iodine vapor.

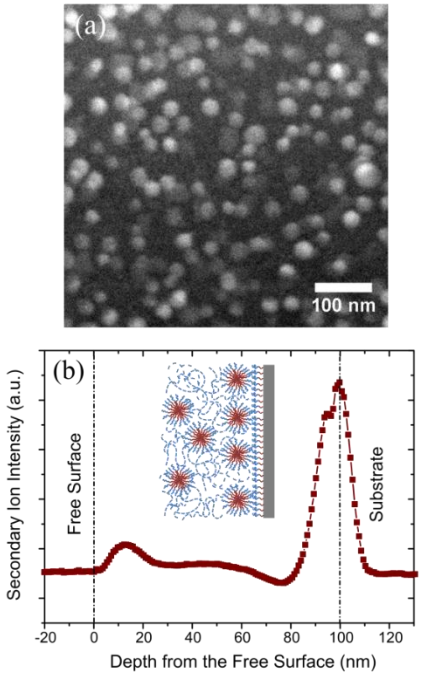

Figure 3 - 1. (a) An STEM image of the P2VP cores of micelles in a PS-b-P2VP/PS(P=6250) mixture (weight ratio of copolymer to homopolymer is 1:4). The sample was annealed in supercritical CO2 at 50 oC, at a pressure of 13.8 MPa for 24 hours (under these conditions the sample is mildly plasticized in order to impart the system sufficient mobility). (b) The DSIMS plot of the depth profile (CN) of P2VP is shown; the inset is a cross sectional schematic of the micelles and the brush-layer at the substrate, based on the STEM and DSIMS data.

The maxima in the depth profile in Figure 3 - 1b are due to the segregation of the micelles (average core diameters of ~28 nm) to interfaces and to the formation of the copolymer brush layer (broken line at 100 nm deep into the sample) at the substrate, as discussed in an earlier publication.[29] This interfacial segregation of the micelles is understood to occur when the host chains are excluded from the micelle coronae ($P>>N_{PS}$). This is the so-called "dry-brush" micelle condition. Micelle segregation excludes the long host chains that would otherwise experience a loss of conformational entropy upon confinement between the micelles. Segregation also minimizes the interfacial area of contact between the coronae and host chains, which further contributes to a reduction of the free energy.

The structure of the PS/PS-*b*-P2VP/NP thin film mixtures is now discussed. It is apparent form Figure 3 - 2 that the case PS(N=10)-Au(4) nanoparticles "decorate" the surfaces of the micelles, whereas the other nanoparticles, PS(N=60)-Au(4) and PS(N=280)-Au(4), do not. The relative locations of the NPs in relation to the centers of the micelle cores may be quantified with using 2D projections of the STEM images.

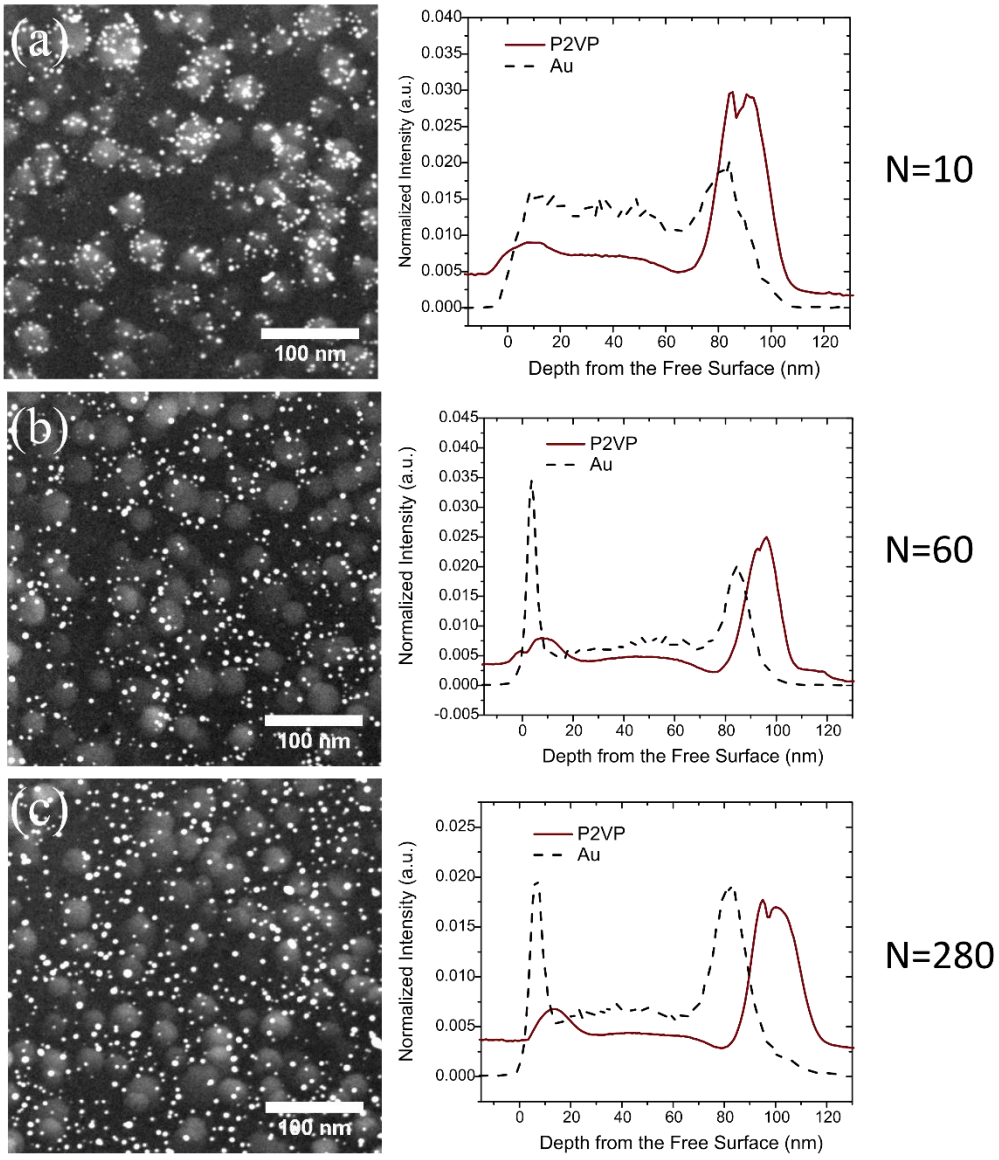

Figure 3 - 2. STEM images and DSIMS (normalized) depth profiles of Au and P2VP in PS-b-P2VP/PS mixtures containing 5 wt% PS(N)-Au(d≈4 nm), with (a) N=10, (b) N=60 and (c) N=280.

Histograms of the normalized distance D between the center of each micelle and the centers of nearby nanoparticles are plotted in Figure 3 - 3; the corresponding STEM images and related schematics are also shown in the same figure. In these histograms, each distance between the center of the NP and the center of a micelle core is normalized by the radius of the micelle core; therefore a value of D=1 is associated with the projection of a NP at the edge of a micelle core. The histogram for the PS(N=10)-Au(4) nanoparticles reveals that more than 70% of the NPs are projected onto the micelles, and at the edges of the micelle cores. We explored the possibility that the NPs are located on the micelle surfaces by estimating the projected locations of particles in a model where particles reside on the surface of a sphere. The details of this calculation are included in Appendix B; our analysis supports the conclusion that most PS(N=10)-Au(4) NPs are located at the surfaces of the micelles. Because micelles, in addition to segregating to the external interfaces, reside within the films, there exists a higher concentration of the PS(N=10)-Au(4) nanoparticles than the PS(N=60)-Au(4) and PS(N=280)-Au(4) nanoparticles, within the interior of the films, due to the fact that most PS(10)-Au(4) nanoparticles "decorate" the surfaces of micelles. Later we will further discuss the reasons the PS(N=10)-Au(d= 4 nm) NPs "decorate" the micelles and why the other NPs , with N>10, remain within the PS hosts, as well as segregate to both external interfaces.

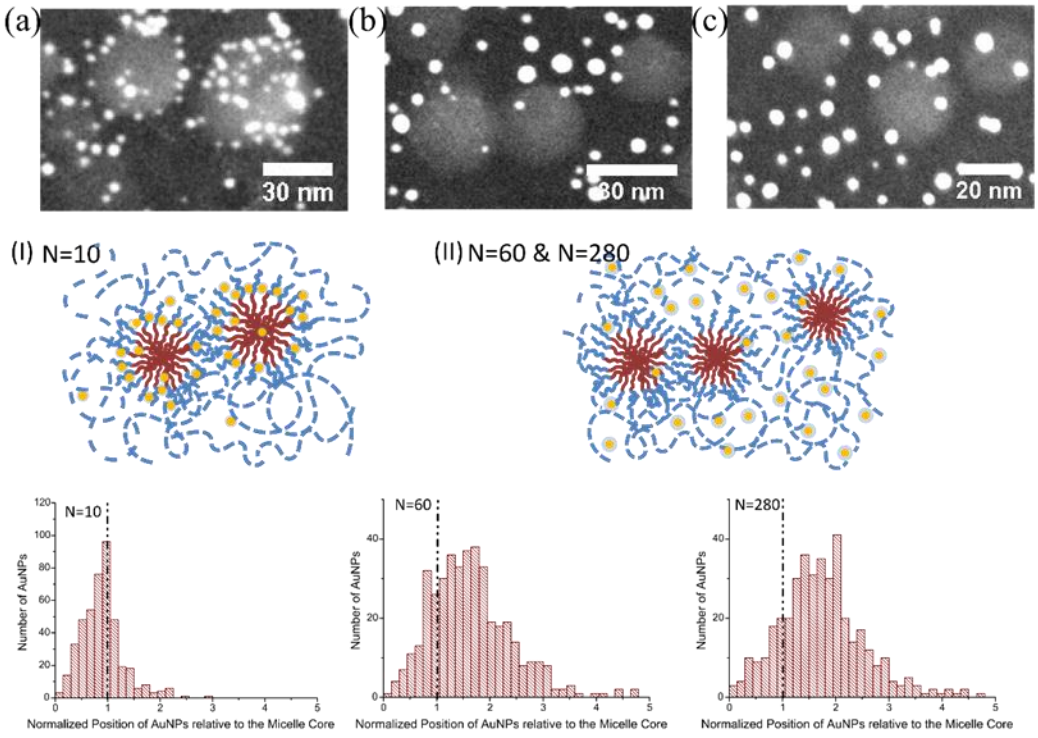

Figure 3 - 3. High magnification STEM images and histograms of nanoparticle positions, D, for the samples described in Figure 2 are shown here. The schematics illustrate 2D projection views of morphologies of the PS(10)-Au(4), PS(60)-Au(4) and PS(280)-Au(4) samples. Since each distance between the NP and the center of micelle core is normalized relative to the radius of micelle core in the histogram, 1 indicates nanoparticles are projected at the micelle core edge and the value larger than 1 indicates nanoparticles located outside the micelle core.

3.3.2. Morphological phase diagram

In the meantime we discuss a morphological diagram of $1/R_c$ versus N, which qualitatively delineates the regimes associated with nanoparticle distributions within the PS-b-P2VP/PS (P=6250) polymer hosts (Figure 3 - 4). For the largest nanoparticles (d=6 nm) onto which the longest chains are grafted (N=280 and N=481), complete phase separation, accompanied by structural instabilities (surface roughening), occurs between the NPs and the

polymer; this is associated with Regime I. For the limiting case N=10 and d=6 nm, NPs are almost completely excluded to the substrate, due to van der Waals attractions with the substrate (Regime III). The situation described earlier, where nanoparticles tethered by sufficient short PS chain (N=10) "decorate" the surfaces of the micelles, is associated with Regime IV. When the curvature of nanoparticles further increases (the smallest nanoparticles), the NPs primarily enrich the free surface (Regime V). Finally in Regime II, the nanoparticles reside at the external interfaces as well as within the PS hosts. The rationale behind the formation of these morphological regimes is discussed in the remainder of this chapter.

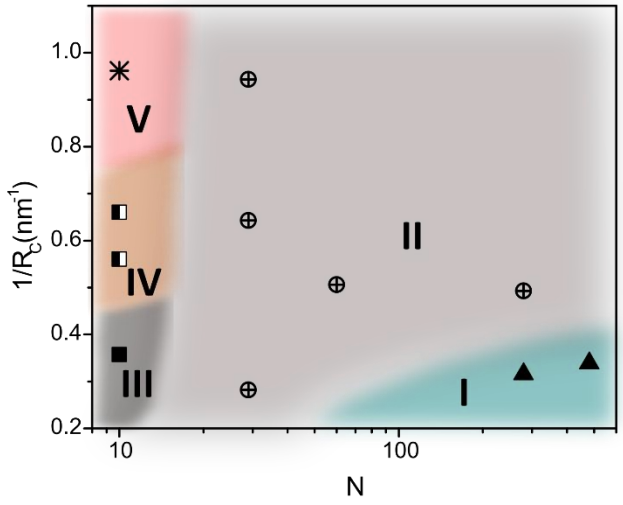

Figure 3 - 4. A morphological diagram of 5 wt% PS-coated nanoparticles in PS-b-P2VP/PS (P=6250, P≫NPS) thin films with micelle structure at relatively constant grafting densities, dependent of the curvature of particle core ~1/RC and grafted chain length N.

3.3.3. Regime I: Phase separation between the NPs and the homopolymer host

Complete phase separation between the NPs and the homopolymer hosts occurs for sufficiently large values of N and R_C. The STEM images of the Au-NPs and the SIMS profiles of Au and P2VP, in Figure 3 - 5a and 5b, respectively, together reveal that the NPs are located preferentially at the free surface and at the substrate. There is however a distinction between details of the phase separation morphologies of two samples. The STEM image in Figure 5b for the PS(N=280)-Au(d=6) sample shows that the NPs form 2D clusters, which is indicative of phase separation between the nanoparticles and the homopolymer PS hosts, as discussed earlier by Kim and Green.[11]

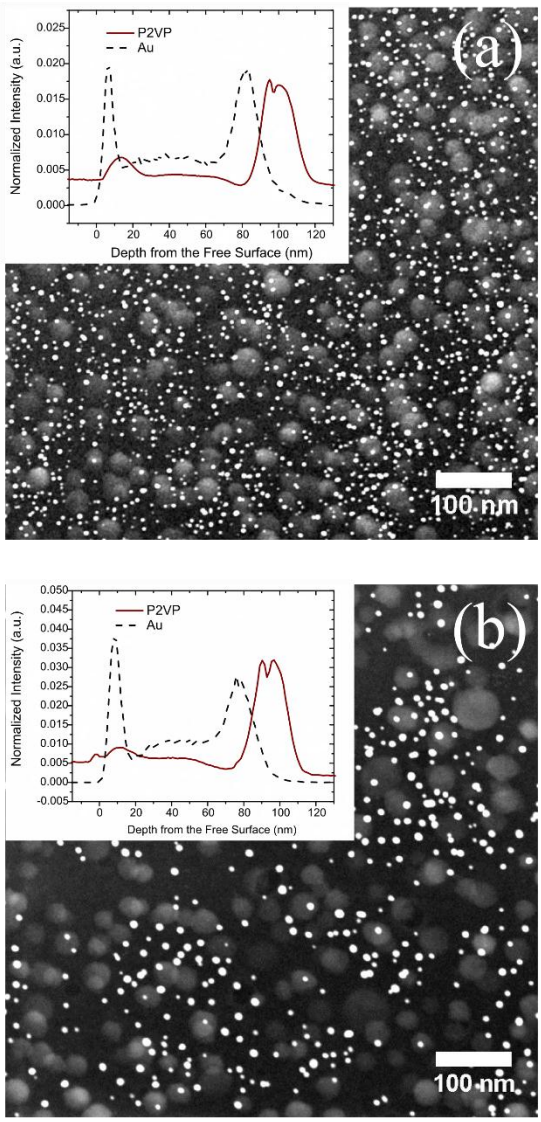

Figure 3 - 5. STEM images of PS-b-P2VP/PS samples containing: (a) 5wt% PS(280)-Au(4) (b) 5wt% PS(280)-Au(6). The insets of (a) and (b) show corresponding DSIMS profiles of Au and P2VP.

This is further explained from the following. In thin films, polymer/polymer phase separation is manifested by the development and growth of surface fluctuations, as one component phase separates and eventually attempts to form droplets on the surface of the other layer.[11,36,37] To this end, we examined the surface topographies of the samples and performed a power spectrum density analysis (PSD) (see Figure 3 - 6a). The PSD maxima and the average frequency of the fluctuations for the PS(N=280)-Au(d=6) sample are significant; they are virtually non-existent for the sample containing the PS(N=280)-Au(d=4) NPs; this manifests a smaller degree of phase separation. It is apparent from the image in Figure 3 - 5b that the nanoparticles exhibit a tendency to form clusters; these nanoparticle clusters denote the peak locations (large local collections) of nanoparticles that form in order to minimize the contact between long chain grafted particles and much longer PS host chains. The PS(280)-Au(4) nanoparticles do not exhibit a tendency to form clusters, which is indicative of a smaller degree of phase separation.

This phase separation may be understood from the following. The brush-coated nanoparticle possesses the structure of a multi-arm star polymer when $N^{1/2}a >> R_C$ (N=280), where *a* is the length of a monomer.[38-40] There exists an excess free energy of mixing between a multi-arm star and linear chains; such mixtures become unstable for sufficiently long chain lengths.[41] The tendency of the tethered nanoparticles to segregate to the free surface and the substrate is generally due to the fact that tethered chains suffer less conformational entropy penalties upon segregation to interfaces than the linear PS host chains of the same degree of polymerization.

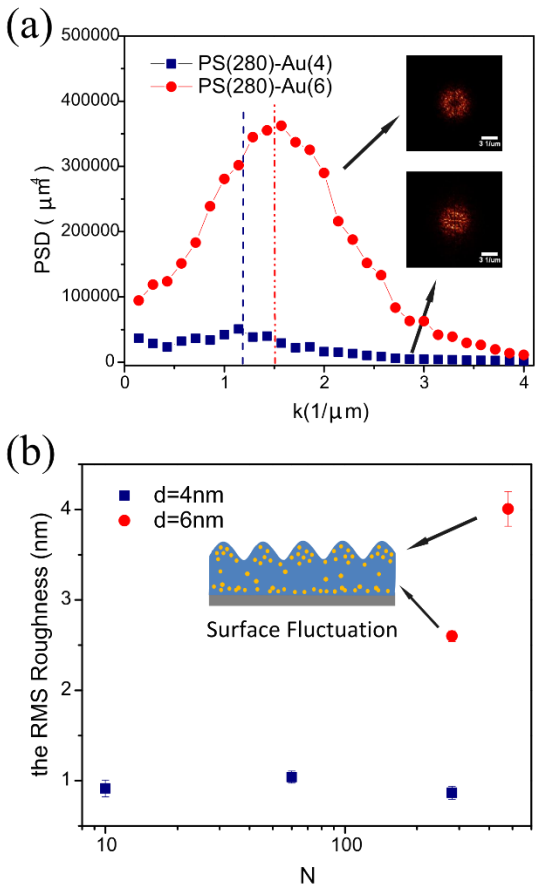

Figure 3 - 6. (a) Power spectral density (PSD) profiles of thin film mixtures containing PS(280)-Au(4) (navy squares) and PS(280)-Au(6) (red circles) nanoparticles. The lines denote the characteristic wave vector of each sample. (b) The root mean square (RMS) roughness determined from topographies for the mixtures containing PS(N)-Au(4) and PS(N)-Au(6). The schematic in the inset of part (b) illustrates the surface fluctuations of PS(280)-Au(6) and PS(481)-Au(6) thin film samples. In order to simplify the drawings, the micelles in the polymer matrix are omitted.

The size and curvature of nanoparticles also plays an important role in miscibility of the system.[6,9,13,14] For a constant grafting density, the effective grafting density decreases with increasing nanoparticle curvature. Hence the grafted chains are less stretched, increased conformational entropy, and the probability of intermixing between the brush and host chains increases, thereby enhancing, comparatively, the miscibility of

nanoparticles in the host chains. The larger nanoparticle core is also associated with a larger driving force for phase separation, for entropic reasons. In light of this there exists a stronger driving force for phase separation of the PS(N=280)-Au(d=6 nm) nanoparticles. We will associate this phase separation process, accompanied by the structural instability (surface fluctuation), with Regime I. The structure of the PS(N=280)-Au(d=4) sample is such that the NPs are distributed throughout the sample with enrichment at external interfaces (the free surface and the substrate) and there is no strong evidence of a structural instability. Later we will associate this behavior with regime II, and discuss the reasons in further detail.

3.3.4. Regimes III and V: Short-chain grafted NPs that preferentially reside at external interfaces

The spatial distribution of nanoparticles, of varying diameters, onto which chains of N=10 are grafted, PS(N=10)-Au(d), are shown in Figure 3 - 7 and Figure 3 - 8. It is evident from Figures Figure 3 - 7d and Figure 3 - 8d that the largest nanoparticles reside primarily at the substrate; this behavior is associated with Regime III. In contrast, the smallest nanoparticles (Figure 3 - 7a and Figure 3 - 8a) are located primarily at the free surface (Regime V). The STEM images (Figure 3 - 7a and 7d) show no evidence of correlations between the locations of the NPs and micelles. These two regimes, III and V, are distinct because the dominant driving forces are different.

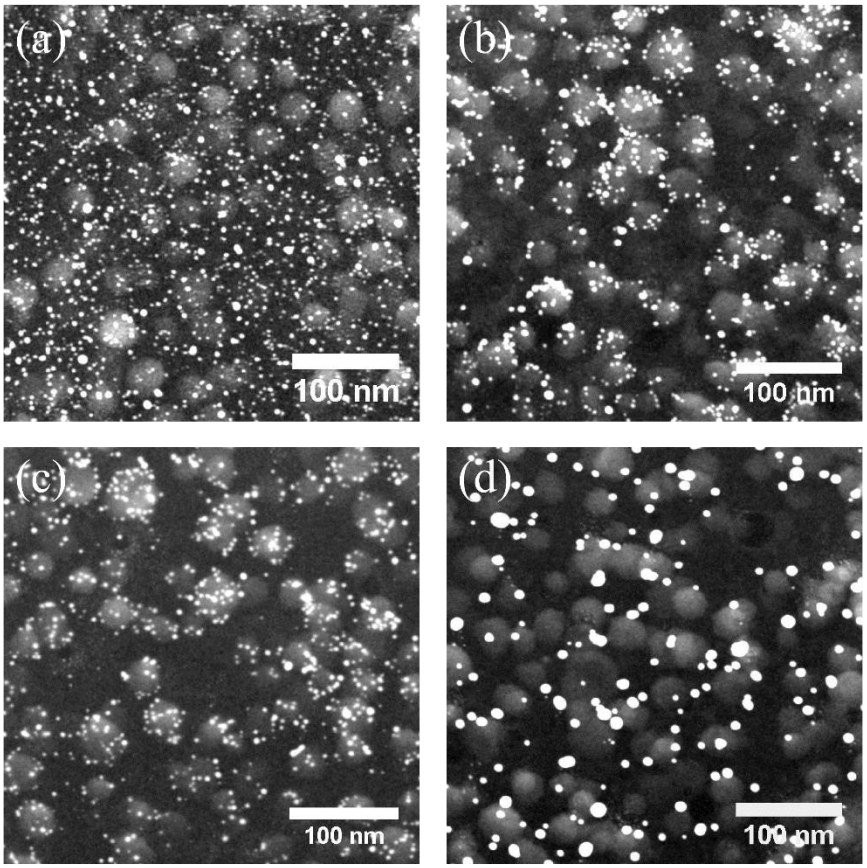

Figure 3 - 7. STEM images are shown for mixtures containing 5 wt% PS(10)-Au(d) nanoparticles with different core diameters: (a) d_{Au} = 2.1nm (b) d_{Au} = 3.0nm (c) d_{Au} = 3.6nm and (d) d_{Au} = 5.6nm.

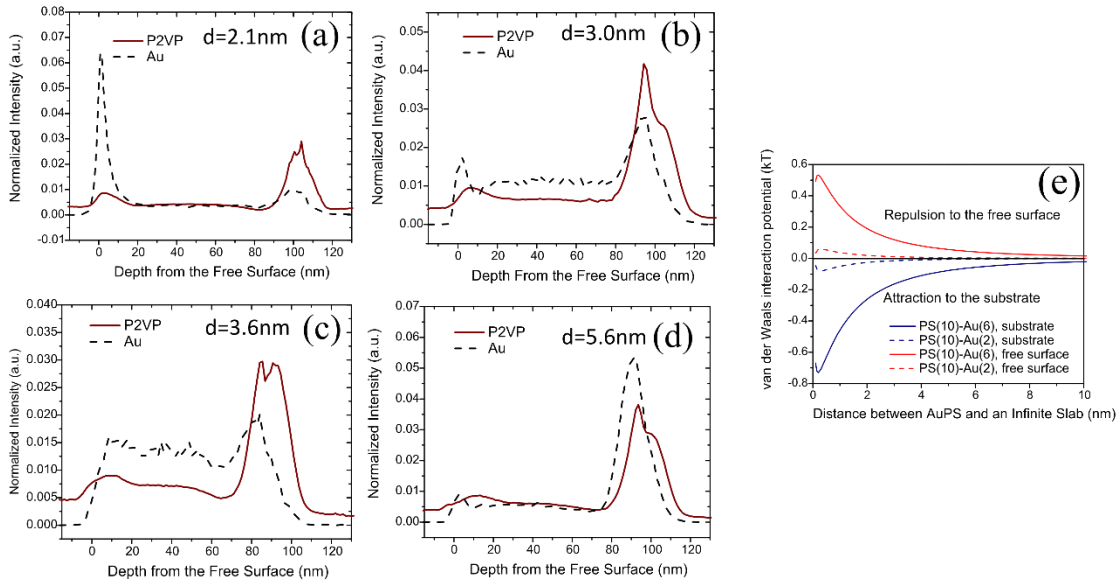

Figure 3 - 8. (a-d) Normalized depth profiles of Au and of P2VP components are shown in for the samples in Figure 7. (e) The long-range non-retarded van der Waals interactions between PS-coated nanoparticles and the substrate or the free surface across the polymer medium were calculated for samples containing PS(10)-Au(2) and PS(10)-Au(6) nanoparticles

The driving forces responsible for the behavior in regimes III and V are now discussed. While the translational entropy, which scales as $1/R_{NP}$, promotes the dispersion of nanoparticles throughout the polymer host,[42,43] the non-retarded long range van der Waals interaction between PS coated gold nanoparticles and the substrate increases with increasing nanoparticle size. The magnitude of the van der Waals interaction may be estimated; the details of the calculation is provided in Appendix B.[44,45] The net attractive interaction between nanoparticles and the Si_3N_4 substrate is plotted in Figure 8e. Our calculations also reveal a net repulsive interaction between nanoparticles and the free surface. Therefore, the approximate calculation of interaction energy is consistent with our observation of the preferential segregation of large particles toward the substrate. The length scale of this

interaction is on the order of a few nm and this interaction decreases with decreasing particle size.

While the translational entropy preferentially favors a homogeneous distribution of the smaller nanoparticles and the van der Waals interactions of these NPs with the external interfaces is weak, these smallest NPs nevertheless exhibited tendency to migrate preferentially to the free surface (regime V). First, a potential driving force for segregation of the smallest nanoparticles to the free surface may be associated with the decrease in adsorption energy of ultra-small particles at the interface between PS block and P2VP block since the adsorption energy at the interface is proportional to the square of particle radius.[46] Secondly, because P>>N, the brush/host chain intermixing is extremely limited. The preferential segregation of nanoparticles to the free surface is accommodated by the gain of conformational entropy of polymer chains that are displaced from the surface.[47,48] This is consistent with that which we observed in NP/homopolymer thin film mixtures.[11,12]

3.3.5. Regime II: NPs distributed throughout the sample with enrichment at external interfaces

In Regime II, the NPs reside at the external interfaces, as well as throughout the PS host. As discussed, the driving forces for preferential segregation to the two external interfaces always exist, so a fraction of the nanoparticles would reside at both interfaces. The van der Waals interactions between the Au cores and the substrate are weaker because the grafted layer is composed of longer chains (N= 60, 280) that contribute to mediating the interaction. These longer chains, in addition, contribute more favorably to mixing with the PS host chains. Hence a fraction of the NPs would remain within the PS host.

3.3.6. Regime IV: NPs reside at the micelle/host interface

Finally, we address the most interesting situation, Regime IV, where the NPs are primarily located in the interfacial region between the edge of micelle cores and the host chains (not within the host). The SIMS profiles in Figure 3 - 8b and 8c show evidence of a significant fraction of NPs within the interior of the films. Additionally, the STEM images in Figure 3 - 7b and 7c reveal that the nanoparticles surround, or "decorate,' the micelles.

Is this phenomenon due to a delicate balance of intermolecular interactions based on the values of R_c, $\sum$, N and P? To examine the former we prepared samples in which the PS host degree of polymerization was reduced to P=125 and other parameters are kept the same. Because of $P<N_{PS}$ under these circumstance, there should be significant intermixing between the PS host chains and the corona chain segments. This is so called "wet-brush" micelles. The information in Figure 3 - 9 reveals that the NPs surround the micelle cores: the 2D STEM images show the particles primarily on the surface of the micelles, the histograms confirm this quantitatively (~70% of nanoparticles are projected on the micelles, in-plane) and the SIMS depth profiles show that the nanoparticle locations mimic the location of the micelle cores. Therefore the fact that the morphology of the samples of vastly different degrees of polymerization of homopolymer PS, suggest that there is a driving force that favors preferential segregation to the micelles, and not to the homopolymer host.

The existence of the adsorption energy at the interface between PS block and P2VP block has been suggested by Kim et al[46,49] under conditions such that gold nanoparticles are coated with sufficiently short PS chains of sufficiently grafting densities since P2VP chains could interact with the Au surfaces, via a long-range interaction.[50] Such an interaction would be largest for the smallest values of N. The other two nanoparticles with much larger N, are

prohibited from coming in proximity to the P2VP core, and therefore cannot absorb to the PS/P2VP interface. Moreover, the larger values of N are also the reason there exists a larger driving force for PS(60)-Au(4) and PS(280)-Au(4) nanoparticles to segregate preferentially to external interfaces in order to avoid the conformational entropy loss of polymer host chains.

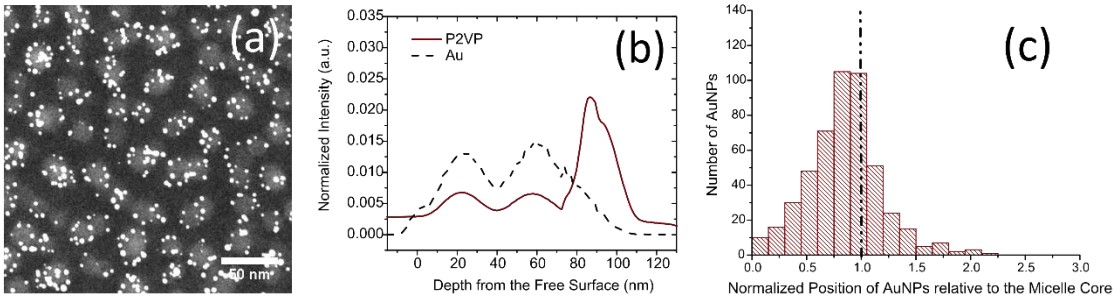

Figure 3 - 9. (a) STEM images (b) DSIMS (normalized) depth profiles of Au and P2VP and (c) histogram of nanoparticle position for PS-b-P2VP/PS (P=125, P<NPS) mixtures containing 5 wt% PS(10)-Au(4)

3.4. Conclusions

We studied the distribution of PS-coated nanoparticles within thin films of micellar copolymer: homopolymer (PS-b-P2VP:PS) blends, supported by Si_3N_4 substrates. The copolymer chains formed micelles (P2VP core/PS corona) in the PS hosts. Based on $1/R_C$ and N, for fixed grafting densities, the spatial distribution of the nanoparticles, driven by competing intermolecular interactions, could be characterized in five different regimes. The distributions include NPs that resided primarily at the free surface or at the substrate, Regimes III and V, respectively, or nanoparticles that primarily surround micelles (Regime

IV). Regime I is associated with phase separation between the brush-coated nanoparticles and the polymer host, accompanied by a structural instability. Finally, nanoparticles at Regime II reside throughout the host with enrichment at external interfaces.

3.5. References

(1) Kim, J.; Yang, H.; Green, P. F. *Langmuir* **2012**, *28*, 9735.
(2) Kumar, S. K.; Jouault, N.; Benicewicz, B.; Neely, T. *Macromolecules* **2013**, *46*, 3199.
(3) Cheng, J. Y.; Ross, C. A.; Chan, V. Z. H.; Thomas, E. L.; Lammertink, R. G. H.; Vancso, G. J. *Adv. Mater.* **2001**, *13*, 1174.
(4) Akcora, P.; Liu, H.; Kumar, S. K.; Moll, J.; Li, Y.; Benicewicz, B. C.; Schadler, L. S.; Acehan, D.; Panagiotopoulos, A. Z.; Pryamitsyn, V.; Ganesan, V.; Ilavsky, J.; Thiyagarajan, P.; Colby, R. H.; Douglas, J. F. *Nature Materials* **2009**, *8*, 354.
(5) Borukhov, I.; Leibler, L. *Macromolecules* **2002**, *35*, 5171.
(6) Chen, X. C.; Green, P. F. *Soft Matter* **2011**, *7*, 1192.
(7) Frischknecht, A. L. *Journal of Chemical Physics* **2008**, *128*.
(8) Frischknecht, A. L.; Hore, M. J. A.; Ford, J.; Composto, R. J. *Macromolecules* **2013**, *46*, 2856.
(9) Green, P. F. *Soft Matter* **2011**, *7*, 7914.
(10) Jancar, J.; Douglas, J. F.; Starr, F. W.; Kumar, S. K.; Cassagnau, P.; Lesser, A. J.; Sternstein, S. S.; Buehler, M. J. *Polymer* **2010**, *51*, 3321.
(11) Kim, J.; Green, P. F. *Macromolecules* **2010**, *43*, 1524.
(12) Meli, L.; Arceo, A.; Green, P. F. *Soft Matter* **2009**, *5*, 533.
(13) Trombly, D. M.; Ganesan, V. *Journal of Chemical Physics* **2010**, *133*.
(14) Ganesan, V.; Ellison, C. J.; Pryamitsyn, V. *Soft Matter* **2010**, *6*, 4010.
(15) Michael, J. A. H.; Russell, J. C. *Macromolecules* **2013**.
(16) Bates, F. S.; Fredrickson, G. H. *Annual Review of Physical Chemistry* **1990**, *41*, 525.
(17) Kim, B.; Fredrickson, G.; Hawker, C.; Kramer, E. *Langmuir* **2007**, *23*, 7804.
(18) Kim, J.; Green, P. F. *Macromolecules* **2010**, *43*, 10452.
(19) Chiu, J. J.; Kim, B. J.; Yi, G. R.; Bang, J.; Kramer, E. J.; Pine, D. J. *Macromolecules* **2007**, *40*, 3361.
(20) Jang, S. G.; Kramer, E. J.; Hawker, C. J. *Journal of the American Chemical Society* **2011**, *133*, 16986.
(21) Kim, B. J.; Bang, J.; Hawker, C. J.; Chiu, J. J.; Pine, D. J.; Jang, S. G.; Yang, S.-M.; Kramer, E. J. *Langmuir* **2007**, *23*, 12693.
(22) Listak, J.; Bockstaller, M. R. *Macromolecules* **2006**, *39*, 5820.
(23) Chen, X. C.; Yang, H. X.; Green, P. F. *Macromolecules* **2011**, *44*, 5758.
(24) Oh, H.; Green, P. F. *Macromolecules* **2008**, *41*, 2561.
(25) Shull, K. R. *Macromolecules* **1993**, *26*, 2346.
(26) Hang, L.; Lang, F.; Qiuming, L.; Jingren, W.; Tianbin, R.; Jianzhong, D. *Polymer Chemistry* **2012**, *3*.
(27) Kaidian, Z.; Qiuming, L.; Jing, C.; Jianzhong, D. *Polymer Chemistry* **2014**, *5*.
(28) Nasongkla, N.; Bey, E.; Ren, J.; Ai, H.; Khemtong, C.; Guthi, J. S.; Chin, S.-F.; Sherry, A. D.; Boothman, D. A.; Gao, J. *Nano Letters* **2006**, *6*, 2427.
(29) Zhao, J.; Chen, X. C.; Green, P. F. *Soft Matter* **2013**, *9*, 6128.
(30) Brust, M.; Walker, M.; Bethell, D.; Schiffrin, D. J.; Whyman, R. *Journal of the Chemical Society-Chemical Communications* **1994**, 801.
(31) Meli, L.; Li, Y.; Lim, K. T.; Johnston, K. P.; Green, P. F. *Macromolecules* **2007**, *40*, 6713.

(32) Tomasko, D. L.; Li, H.; Liu, D.; Han, X.; Wingert, M. J.; Lee, L. J.; Koelling, K. W. *Industrial & Engineering Chemistry Research* **2003**, *42*, 6431.
(33) Horcas, I.; Fernández, R.; Gómez-Rodríguez, J. M.; Colchero, J.; Gómez-Herrero, J.; Baro, A. M. *Review of Scientific Instruments* **2007**, *78*.
(34) Ferreira, P. G.; Ajdari, A.; Leibler, L. *Macromolecules* **1998**, *31*, 3994.
(35) Matsen, M. W.; Gardiner, J. M. *Journal of Chemical Physics* **2001**, *115*, 2794.
(36) Jandt, K. D.; Heier, J.; Bates, F. S.; Kramer, E. J. *Langmuir* **1996**, *12*, 3716.
(37) Wang, H.; Composto, R. J. *Journal of Chemical Physics* **2000**, *113*, 10386.
(38) Klos, J.; Pakula, T. *Journal of Chemical Physics* **2003**, *118*, 7682.
(39) Klos, J.; Pakula, T. *Macromolecules* **2004**, *37*, 8145.
(40) Xu, J.; Qiu, F.; Zhang, H.; Yang, Y. *Journal of Polymer Science Part B-Polymer Physics* **2006**, *44*, 2811.
(41) Fredrickson, G. H.; Liu, A. J.; Bates, F. S. *Macromolecules* **1994**, *27*, 2503.
(42) Lee, J. Y.; Buxton, G. A.; Balazs, A. C. *Journal of Chemical Physics* **2004**, *121*, 5531.
(43) Lee, J. Y.; Shou, Z. Y.; Balazs, A. C. *Macromolecules* **2003**, *36*, 7730.
(44) Israelachvili, J. N. In *Intermolecular and Surface Forces (Third Edition)*; Israelachvili, J. N., Ed.; Academic Press: San Diego, 2011, p 253.
(45) Nir, S. *Progress in Surface Science* **1977**, *8*, 1.
(46) Bumjoon, J. K.; Glenn, H. F.; Edward, J. K. *Macromolecules* **2008**, *41*.
(47) McGarrity, E. S.; Frischknecht, A. L.; Frink, L. J. D.; Mackay, M. E. *Physical Review Letters* **2007**, *99*.
(48) McGarrity, E. S.; Frischknecht, A. L.; Mackay, M. E. *Journal of Chemical Physics* **2008**, *128*.
(49) Bumjoon, J. K.; Joona, B.; Craig, J. H.; Edward, J. K. *Macromolecules* **2006**, *39*.
(50) Martin, S. K.; Kenneth, R. S.; Andrew, J. K. *Journal of Applied Physics* **1992**, *72*.

CHAPTER 4.
PHASE BEHAVIORS OF DIBLOCK COPOLYMER/STAR-SHAPED POLYMER THIN FILM MIXTURES

4.1. Introduction

Thin film polymer blends continue to garner much interest due to the fact that their surface properties can be tailored for various applications, such as smart coatings, enhancement of wetting and lubricants. This has motivated a lot of fundamental studies on the phase behaviors and surface composition of polymer blends.[1-7] Preferential segregation of the components of a blend is universal phenomenon in all polymer blends, and is responsible for composition gradients near surfaces (this is typically the lowest cohesive energy density component); in some cases the segregation would be responsible for inducing phase separation in blends at significantly different temperatures from the bulk.[8,9] The driving force governing surface segregation effects is related to entropic effects and especially to differences between the cohesive energy densities of the constituent polymers. It is therefore possible to exploit this phenomenon for materials design.

In A/B miscible homopolymer blends, surface composition is dominated by the lower surface tension component in the absence of unusual entropic effects; this contributes to decreasing the free energy of the system.[10,11] The phase behavior of these systems is well

understood, including the phenomenon surface-directed spinodal decomposition.[12] It occurs when the attraction of one component to the surface breaks the symmetry. As a result, the shape of the coexistence curve is changed, due to preferential interfacial wetting of one component.

Apart from changing chemistries of components in polymer blends, changing architectures is another well-known strategy to tune the composition profile of polymer blends. In binary blends of linear/star-shaped polymer of identical chemistry, star-shaped polymers are found to enrich the surface due to their lower surface tension, which is associated with a high number of chain ends and related entropic effects.[13] Polymer chains experience a great configurational entropy penalty than the ends residing at the surface. The linear response theory predicts that the surface tension of star-shaped polymers decreases with increasing number of arms f and decreasing number molecular weight.[3,13] Much attention is also paid on the phase behaviors of these systems because of the important roles on the surface properties. The theoretical study predicts that entropic driven phase separation tends to occur when star-shaped polymer has a sufficient high f.[1,14]

Of particular interest in this work, we utilize star-shaped polymer to control phase behaviors and in turn surface composition of thin film diblock copolymer (BCP)/star-shaped polymer blends. It is well known that BCPs as a minor component in linear homopolymer hosts, exhibiting significant interfacial activities, self-assemble into micelle structures of different geometries.[15-21] Recently our group showed that polystyrene-b-poly (2-vinylpyridine) (PS-b-P2VP) self-organized into spherical micelles with an inner core of P2VP and an outer corona of PS in linear PS thin films. The average diameter of micelle core increased with the degree of polymerization of the linear PS host P and reached a plateau at large P. Within the large P regime, micelles self-organized into close packed structure and

migrated to the free surface.[20] Surprisingly, nothing has been done on the thermodynamics of BCP/ star-shaped homopolymer system.

Herein, the phase behavior and surface composition of BCP/star-shaped polymer blends is examined in supported PS-b-P2VP/star PS thin film mixtures. In such mixtures, the minor component PS-b-P2VP behaves like in the linear PS hosts and, also forms spherical micelles composed of an inner core of P2VP block and an outer corona of PS block. The dispersion or phase separation of micelles in star PS hosts are largely dictated by the extent of intermixing of corona chains with star PS hosts. In the star PS host of a sufficiently high *f* and small arm molecular weight M_n^{arm}, close-packed micelles segregate near the substrate, leaving the area near the surface with BCP depletion in contrast to the segregation of micelles to the free surface in long linear PS hosts; the star PS-rich surface is dominated by its lower surface energy. As M_n^{arm} increases, the crossover of micelle segregation from the substrate to the free surface is observed; this is manifested by the transition of star PS from soft colloidal-like to linear-like behavior.

4.2. Experimental Section

A series of star-shaped polystyrene, with different functionalities and different molecular weight were synthesized by means of anionic polymerization using high vacuum techniques.[25,26] The star-shaped macromolecules used in this study are described in Table 1.

The diblock copolymer (BCP) polystyrene-b-poly(2-vinylpyridine) (PS-b-P2VP, Mn(PS) = 50,900 g/mol, degree of polymerization of PS block NPS =489 and Mn(P2VP)=29,100 g/mol, degree of polymerization of P2VP block NP2VP=277, polymer Source Inc) and various star PS were dissolved in toluene separately and mixed such that the

weight ratio of PS-b-P2VP to star PS was 1:4. The polymer blend thin films were prepared by spin-coating mixture solutions onto cleaned silicon substrates with native oxide layer (WaferNet, Inc.). The films were subsequently dried in vacuum at 65 °C overnight and annealed at 160 °C for 24 hours. The thicknesses of the annealed films were 105 ± 5 nm, which were determined using spectroscopic ellipsometer (J.A. Woollam CO.).

Scanning transmission electron microscopy (STEM) was performed using the JOEL 2010F instrument, equipped with a high angle annular dark field (HAADF) detector (Z-contrast), to characterize the formation of micelles in thin films. Prior to the STEM measurement, the films were stained in iodine vapor for 10 min. The quantitative analysis of micelles was performed using imageJ and summarized in Table 4 - 1. More than 200 micelles from 3 to 4 different areas were analyzed in order to make sure that the information discerned from the samples were representative of the behavior for each film. The depth profiles of copolymer in the films were obtained using dynamic secondary ion mass spectroscopy (DSIMS, Cameca IMS 7f).

Table 4 - 1. The characteristics of star-shaped polystyrene (PS) and diblock copolymer micelle in corresponding hosts

Star PS host	Number of arms, f[a]	M_n^{arm} (kg/mol)[b]	Surface tension, Υ (mJ/m^2)	Diameter of micelle core, D_{core} (nm)	Number density of micelles, $n_{micelle}$ (μm^{-3})
4-7k	4	7	29.9	25.5 ± 4.4	4560 ± 310
16-14k	16	14	29.2	37.5 ± 3.3	1705 ± 115
64-9k	64	9	28.5	45.9 ± 5.1	840 ± 135
64-36k	64	36	30.2	37.8 ± 3.2	1465 ± 75
64-140k	64	140	30.7	40.6 ± 8.1	1220 ± 45

[a]Number of arms, *f*, determined by the ratio M_w^{star}/M_n^{arm}; [b]From membrane osmometry in toluene at 35°C.

4.3. Results and Discussion

The formation of BCP micelles in short arm star-polymer hosts of various *f* (*f*=4, 16 and 64, see Table 4 - 1) is evident from STEM images shown in Figure 4 - 1. STEM images of 20% PS-b-P2VP in star polystyrene hosts of (a) 4-7k, (b) 16-14k (c) 64-9k. All films were 105±5nm.. In these images, the P2VP cores appear to be bright, due to selectively staining by iodine vapor. The diameter of micelle cores, D_{core} and number density of micelles, $n_{micelle}$ for each sample are calculated and reported in Table 4 - 1. The characteristics of star-shaped polystyrene (PS) and diblock copolymer micelle in corresponding hosts. Three things are clearly shown from Table 4 - 1 and Figure 4 - 1: (1) D_{core} increases with increasing *f*; (2) $n_{micelle}$ decreases accompanying the increase in D_{core} with increasing *f*; (3) in 64-9k host, the organization of large micelles exhibits hexagonally close-packed aggregation.

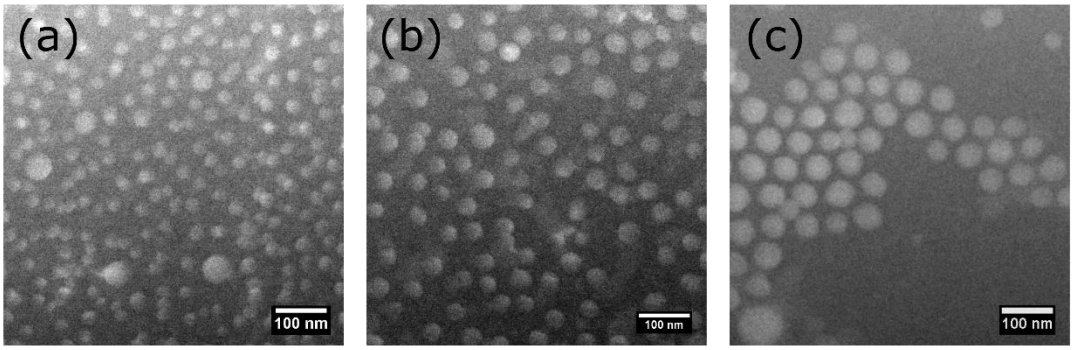

Figure 4 - 1. STEM images of 20% PS-b-P2VP in star polystyrene hosts of (a) 4-7k, (b) 16-14k (c) 64-9k. All films were 105±5nm.

SIMS was used to qualitatively determine the concentration profile of BCP in star PS thin film mixtures. The SIMS experiments measured the CN group concentration of P2VP,

which provides direct information about the concentration profile of the P2VP block and thus BCP chains. The thickness of each film was normalized such that 0 represents the free surface and 1 represents the substrate. For all samples, the sharp peaks at the substrate indicate the formation of brush layer as discussed in our prior publication.[20,21] Except for the peak associated with the brush layer, SIMS data plotted in Figure 4 - 2 reveal a drastic difference in the concentration profile of BCP chains by varying *f* of star polymers. For the star PS host of 4-7k, two distinguishable peaks show two layers of micelles uniformly distributed throughout the film; this reflects the composition near the surface of the film is a mixture of BCP and star PS. For the case of $f = 16$, two peaks become largely overlapped and tend to migrate toward the substrate compared to that in the case of $f = 4$ and thus concentration of BCP near the surface is reduced. For the case of $f = 64$, there is only one broad peak adjacent to the brush layer at the substrate; this reveals that large micelles in star PS host of sufficiently high *f* preferentially segregate towards near the substrate and thus the surface is star polymer rich with depletion of BCP chains. It is worthwhile to note that, in the linear PS of equivalent or larger total molecular weight BCP micelles segregate to the free surface.

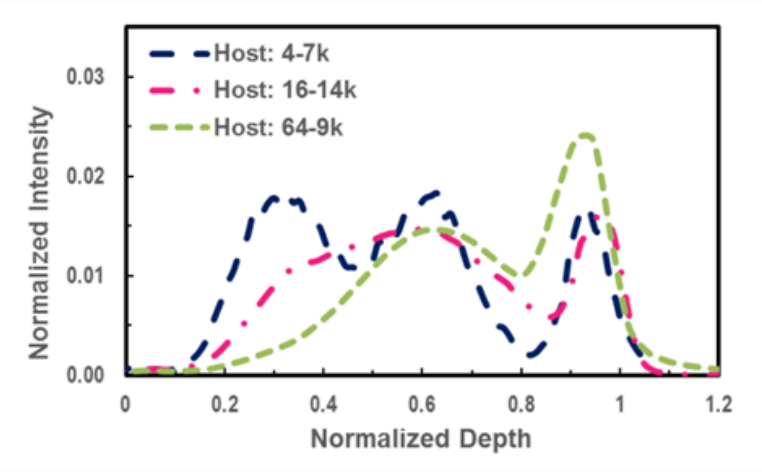

Figure 4 - 2. Depth profiles of P2VP components in star polystyrene hosts of 4-7k (long dash line), 16-14k (dot-dash line) and 64-9k (short dash line) measured by SIMS

The change in the concentration of BCP near the surface of BCP/star PS thin film mixtures by varying the functionality *f* of star PS described above, can be understood in part by considering the entropic interaction on the formation of micelles in star-shaped polymers. With regard to the linear PS host, the change in D_{core} is associated with the conformational entropy cost of mixing between corona chains and host chains. Simulations and theory reveal the nature of star-shaped polymer: the chain segments close to the star polymer cores are more stretched due to topology and related entropic effects.[22,23] This creates a gradient in monomer density from the vicinity of the core to the chain ends and the effect increases with increasing *f* or decreasing M_n^{arm}. The local monomer packing would influence the stretching of polymer chains close to the star-polymer cores and thus interpenetration of neighboring molecules. In the sample containing star host of 4-7k, the star host chains of sufficiently small *f* behave like short linear PS and readily intermix with the corona chains of micelles in order to gain translational entropy. As a result of intermixing, the PS corona are

stretched and the P2VP cores are concurrently compressed in order to maintain constant segmental density. Smaller micelles are more uniformly distributed throughout the film to gain translational entropy and consequently the film surface is composed of a mixture of BCP chains and star polymer. As *f* increases, the extent of intermixing with star host would largely decrease. In the star PS host of 64-9k environment, the star polymer chains of sufficiently high *f* and small M_n^{arm}, are largely excluded from the corona chains since they experienced entropic penalty when confined within corona chains. Moreover, 64-9k star host chains migrate from between corona chains, leading the formation of close-packed micellar structure; this further minimizes the corona/star host interaction. The overall entropic gain drives micelles to reside at the interfaces. However, the entropic argument cannot explain the segregation of micelles toward the substrate (surface depletion of BCP chains) in 64-9k star host instead of segregation to the free surface (surface excess of BCP chains) like their linear analog.

We explore the possibility of surface depletion of BCP chains in star polymer hosts due to lower surface energy of star polymers. Archer and coworkers used linear response theory to show that the surface tension of star-shaped polymer can be reasonably described by the equation: $\gamma(M_n) = \gamma(\infty) + \rho RT(fU^e + U^j)/M_n$.[3,13] In this equation, $\Upsilon(\infty)$ is the surface tension for infinite number-average molecular weight, ϱ is the bulk density, R is the universal gas constant, T is temperature. U^e represents the effective attractive interaction of chain ends to the surface and U^j represents the effective repulsion of branch points to the surface. The estimated Υ for star PS hosts at 160 °C are listed in Table 1. For surface tension of corona PS, we used the surface tension of linear PS Υ_L = 30.1 mJ/m^2 at 160 °C.[24] In polymer blends thin film, there is always surface excess of the component with lower surface energy. The progressively lower surface tensions of star PS with increasing *f* can account for

the decreased surface concentration of BCP chains discussed earlier. This is consistent with our result that micelles segregate toward the substrate in the star PS host of sufficiently high *f* and small M_n^{arm}, leading to the formation of surface layer with BCP depletion. One might surmise that because $\Upsilon(4\text{-}7k) < \Upsilon_L$, the early observation that micelles (BCP chains) are uniformly distributed in 4-7k host would be contradictory. This can be easily understood that entropic gain due to intermixing overcomes the effect of slight difference in surface tension between two components.

The phase separation of micelles in the star host of sufficiently high *f* and small M_n^{arm} is enhanced in comparison with that in long linear hosts. In the star host of 64-9k, the average edge-to-edge distance of micelle core d, between the neighboring micelles in a micelle aggregate determined from STEM images, assuming d = 2h = 13.2 nm where h is the thickness of micelle corona; Theoretically, under the assumption of unperturbed coronae, h_o = 10.1 nm calculated on the basis of D_{core} = 45.9 nm shown in Table 1. Hence we can see $d < 2h_o$ in contrast to $d > 2h_o$ (d = 20.5nm and h_o = 8.9 nm)[21] in long linear PS hosts. Recall that in long linear PS hosts, although long host chains are excluded from the corona chains, there is always some degree of intermixing between the host and the outer part of the corona. As a result, $d > 2h_o$ in long linear PS hosts. In this work, $d < 2h_o$ indicates the intermixing of corona chains between neighboring micelles in order to minimize contact with soft colloidal like star host. This also can be reflected by the fact that there is larger average number of micelles per aggregate in star PS host of 64-9k than that in their linear analogous with equivalent or larger total molecular weight. In linear/star polymer blends, phase separation has been predicted when *f* is sufficiently large.[1,14] Clearly, phase separation is more favorable in coronae (equivalent to grafted chains)/star PS mixtures because of conformational

entropic loss associated with stretching of corona chains and rearrangement of star PS like soft colloids at the outer part of coronae.

To further probe the role of star PS toward determining the phase behaviors of our systems, additional blends were examined. Figure 4 - 3 shows the concentration profile of BCP chains in 64-arm star PS of different M_n^{arm}. Apart from the sharp peak for the brush layer mentioned earlier, the strong broad peak transits from near the substrate to the free surface, indicating the crossover of micelles segregation from the substrate to the free surface when M_n^{arm} increases from 9k to 140k. The depth profiles of BCP can be readily understood by invoking surface tension arguments: transition of surface composition from BCP depletion to BCP excess is driven by change in Υ of star-shaped polymer. Υ increases with increasing M_n^{arm} for a given f = 64 and the crossover to $\Upsilon > \Upsilon_L$ occurs at M_n^{arm} = 31kg/mol. One may notice there is a shoulder in the interior next to the surface peak in the case of 64-140k host. This implies that there is some extent of intermixing corona chains with 64-140k star host chains, which is also evident from STEM images shown in Figure 4 - 4. The sizes of micelle cores formed in the star PS hosts of 64-36k and 64-140k are slightly smaller than those formed in the star host of 64-9k (Table 1) and the close-packed structure disappears as M_n^{arm} increases.

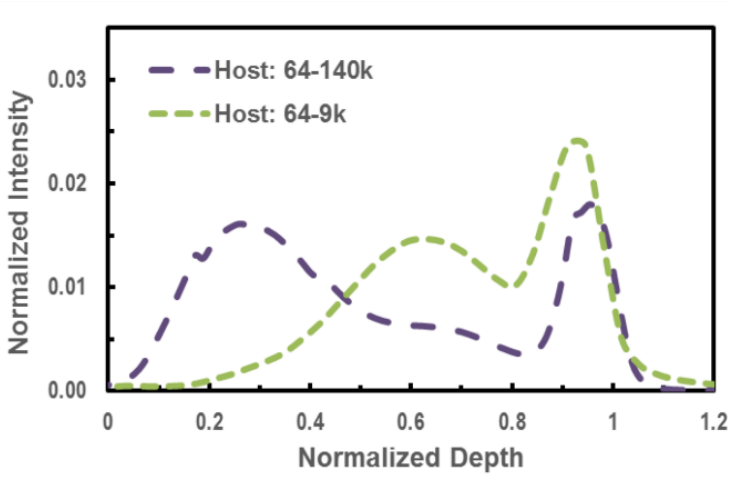

Figure 4 - 3. Depth profiles of P2VP components in star polystyrene hosts of 64-140k (long dash line) and 64-9k (short dash line) measured by SIMS

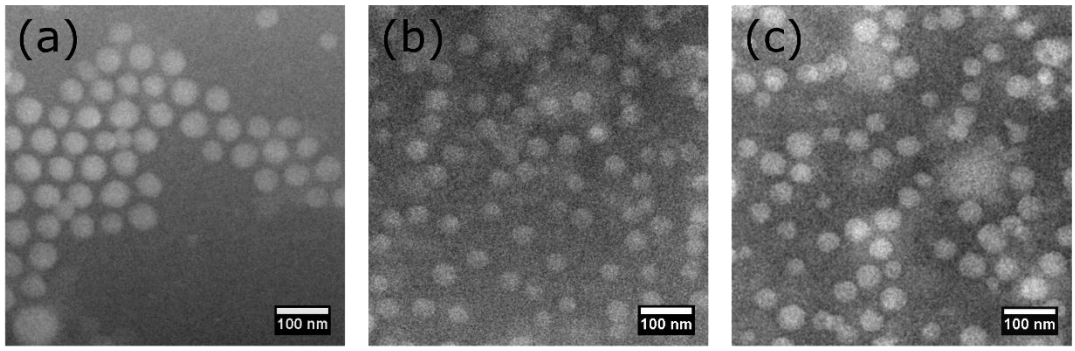

Figure 4 - 4. STEM images of 20% PS-b-P2VP in star polystyrene hosts of (a) 64-9k, (b) 64-36k (c) 64-140k

4.4. Conclusions

In conclusion, we showed how the functionality, and arm lengths of star-shaped polymers control the phase behaviors of BCP/star-shaped polymer thin film mixtures. The BCPs form micelles within the star-shaped polymer hosts. Clearly, the system can be tailored

to exhibit miscibility or phase separation of micelles in star-shaped polymer hosts and the resultant composition profiles near the surface showed variations in BCP concentration, ranging from BCP depletion to BCP excess; this cannot be achieved in their linear analog system. The balance of the surface energy of star-shaped polymers and the entropic interaction associated with intermixing between corona blocks and star-shaped polymers would be responsible for the behaviors reported here. The implications of these results are that changing the architecture of polymers and their chain lengths, but without changing the chemistry of polymers, can significantly affect the thermodynamics of the mixture and particularly the interfacial composition.

4.5. References

(1) Fredrickson, G. H.; Liu, A. J.; Bates, F. S. *Macromolecules* 1994, *27*, 2503.
(2) Chen, Y. Y.; Lodge, T. P.; Bates, F. S. *Journal of Polymer Science Part B-Polymer Physics* 2000, *38*, 2965.
(3) Minnikanti, V. S.; Archer, L. A. *Journal of Chemical Physics* 2005, *123*.
(4) Qian, Z. Y.; Minnikanti, V. S.; Archer, L. A. *Journal of Polymer Science Part B-Polymer Physics* 2008, *46*, 1788.
(5) Xu, L.; Yu, X. F.; Shi, T. F.; An, L. J. *Macromolecules* 2008, *41*, 21.
(6) Jones, R. L.; Indrakanti, A.; Briber, R. M.; Muller, M.; Kumar, S. K. *Macromolecules* 2004, *37*, 6676.
(7) Minnikanti, V. S.; Archer, L. A. *Macromolecules* 2006, *39*, 7718.
(8) Jones, R. A. L.; Kramer, E. J. *Polymer* 1993, *34*, 115.
(9) Elman, J. F.; Johs, B. D.; Long, T. E.; Koberstein, J. T. *Macromolecules* 1994, *27*, 5341.
(10) Nakanishi, H.; Pincus, P. *Journal of Chemical Physics* 1983, *79*, 997.
(11) Schmidt, I.; Binder, K. *Journal De Physique* 1985, *46*, 1631.
(12) Jones, R. A. L.; Norton, L. J.; Kramer, E. J.; Bates, F. S.; Wiltzius, P. *Physical Review Letters* 1991, *66*, 1326.
(13) Qian, Z.; Minnikanti, V. S.; Sauer, B. B.; Dee, G. T.; Archer, L. A. *Macromolecules* 2008, *41*, 5007.
(14) Camargo, M.; Likos, C. N. *Journal of Chemical Physics* 2009, *130*.
(15) Shull, K. R.; Winey, K. I.; Thomas, E. L.; Kramer, E. J. *Macromolecules* 1991, *24*, 2748.
(16) Akiyama, M.; Jamieson, A. M. *Polymer* 1992, *33*, 3582.
(17) Semenov, A. N. *Macromolecules* 1992, *25*, 4967.
(18) Esselink, F. J.; Semenov, A. N.; Tenbrinke, G.; Hadziioannou, G.; Oostergetel, G. T. *Physical Review B* 1993, *48*, 13451.
(19) Ruzette, A. V.; Leibler, L. *Nat. Mater.* 2005, *4*, 19.
(20) Chen, X. C.; Yang, H. X.; Green, P. F. *Macromolecules* 2011, *44*, 5758.
(21) Chen, X. C.; Yang, H. X.; Green, P. F. *Macromolecules* 2012, *45*, 3993.
(22) Likos, C. N.; Lowen, H.; Watzlawek, M.; Abbas, B.; Jucknischke, O.; Allgaier, J.; Richter, D. *Physical Review Letters* 1998, *80*, 4450.
(23) Vlassopoulos, D.; Fytas, G.; Pakula, T.; Roovers, J. *Journal of Physics-Condensed Matter* 2001, *13*, R855.
(24) Dee, G. T.; Sauer, B. B. *Journal of Colloid and Interface Science* 1992, *152*, 85.
(25) Hadjichristidis, N.; Iatrou, H.; Pispas, S.; Pitsikalis, M. *Journal of Polymer Science Part a-Polymer Chemistry* 2000, *38*, 3211.
(26) Uhrig, D.; Mays, J. W. *Journal of Polymer Science Part a-Polymer Chemistry* 2005, *43*, 6179.

CHAPTER 5.
CONCLUSIONS AND RECOMMENDATIONS FOR FUTURE WORK

This dissertation demonstrated the phase behaviors and morphological design of thin film multi-component polymeric systems, including polymer nanocomposites and polymer blends. Different morphological structures were obtained by understanding and controlling intermolecular interactions between the constituents of the mixtures. This final chapter includes two parts, summary of the key findings of this research work and recommendations for future work.

5.1. Conclusions

5.1.1. Morphological design in nanoparticles/diblock copolymer/homopolymer thin film systems

We investigated the morphologies of thin film AuNPs/BCP/homopolymer system in which AuNPs were end-tethered with PS or P2VP. The PS-b-P2VP chains, in addition to forming a brush layer at the substrate, also form micelles, composed of inner cores of the P2VP segments and outer coronas of the PS blocks, within the PS hosts. The relative interactions between the NPs and the PS and P2VP-components, together with entropic

interactions and interfacial interactions, generally determine the spatial organization of NPs throughout the thin film polymer blends.

In chapter 2, P2VP grafted NPs were encapsulated within micelle cores, which are evident from STEM images and SIMS profiles. It is noticed that on average each micelle contained one or no NP. In comparison to pure PS-b-P2VP/PS blends, the NP/PS-b-P2VP/PS blends possessed a higher density of, on average, smaller micelles especially when the PS homopolymer chain length was large compared to the corona chain length. This occurred in order to maximize the NP/micelle core interactions (reducing the enthalpy cost) and to maximize the translational entropy of the NPs and the micelles. This sample fabrication procedure is straightforward and compliments the current "toolbox" used to create functional materials from BCP/NP systems.

In Chapter 3, the spatial distribution of PS-grafted Au NPs within this thin film PS-b-P2VP/PS (P >> NPS) system is characterized by a morphological diagram of the curvature of the Au cores, 1/R, vs. the degree of polymerization N of the grafted PS chains. The distribution is quantified by five basic regimes, largely dictated by competing entropic and enthalpic intermolecular interactions. For the largest nanoparticles (2R=6 nm) onto which the longest chains are grafted (N=280 and N=481), complete phase separation, accompanied by structural instabilities (surface roughening), occurred between the NPs and the polymer; this is associated with Regime I. For the limiting case of N=10 and 2R=6 nm, NPs were almost completely excluded to the substrate, due to van der Waals attractions with the substrate (Regime III). The intermediate size nanoparticles tethered by sufficient short PS chain (N=10) "decorated" the surfaces of the micelles, is associated with Regime IV. When the curvature of nanoparticles further increased (the smallest nanoparticles), the NPs

primarily enriched the free surface (Regime V). Finally in Regime II, the nanoparticles resided at the external interfaces as well as within the PS hosts.

5.1.2. Phase behaviors of diblock copolymer/star-shaped polymers

The study in chapter 4 was designed to elucidate the role of star-shaped polymers on the phase behaviors of BCP/star-shaped polymer thin film mixtures. The addition of the low concentration of BCP PS-b-P2VP (20%)in star-shaped PS also results in the formation of micelles composed of an inner core of P2VP block and an outer corona of PS block, like that in the linear PS hosts discussed in the earlier chapters. Miscibility or phase separation of micelles can be tailored by varying number of arms *f* and arm molecular weight M_n^{arm} of star PS hosts. In the star PS of sufficiently large *f* and small M_n^{arm}, close-packed micelles segregated near the substrate in contrast to micelle segregation to the free surface in their linear analog; the resultant BCP depletion near the surface was dominated by the lower surface energy of star PS. For the given large *f*, it is observed that the crossover from micelle segregation towards the substrate to that towards the surface with increasing M_n^{arm} , which is manifested by star PS transition from soft colloid-like to linear-like behaviors. BCP/star-shaped polymer with well controlled phase behaviors can serve as templates for NP organization.

5.2. Recommendations for Future Work

In chapter 2, it is shown that P2VP grafted nanoparticles (degree of polymerization of P2VP grafted chain, N_{P2VP}= 12 and diameter of gold NP core, 2R = 6nm) were sequestered into micelle cores regardless of host chain P due to the enthalpic gain. Each micelle on average contained one or no NP. One can explore the encapsulation conditions

by expanding the parameter space studied to include grafted chain length of P2VP and NP size. These parameters are expected to change the strength of favorable intermolecular interaction between gold and P2VP core and thus affect encapsulation behaviors (e.g. frustration of encapsulation or more than one NPs per micelle). Followed by these experiments, it would be interesting to study the chain relaxation dynamics of the micelle core in the system with different NP encapsulation situations since chain relaxation dynamics of PNCs are profoundly influenced by polymer-NP interactions.

In chapter 3, we developed the morphological diagram to identify the distribution of PS grafted AuNPs in PS-b-P2VP/PS thin film mixtures. In regime II, short PS chain grafted AuNPs of intermediate size "decorated" the surface of micelle cores because of dominant intermolecular interaction between micelle cores and gold surface. This result indicates that we precisely positioned nanoparticles at the interface between two dissimilar polymers, which exhibit surfactant-like behaviors. Adopting this behavior, one can intentionally use such "surfactant particles" to modify the phase behaviors of polymer blends. For example, as we increased nanoparticle concentration from 5 wt% (shown in chapter 3) to 20 wt% (shown in **Error! Reference source not found.**), it is observed that micelle are distorted and connected instead of individual spherical micelles. With increasing concentration of such "surfactant particles", one may possibly create bicontinuous structures which has large interfacial areas between the constituents. The concept of this sample fabrication method involving "surfactant particles" can be applied to create bulk heterojunction organic solar cells, which can effectively enlarge donor/acceptor interfacial area that is responsible for device efficiency.

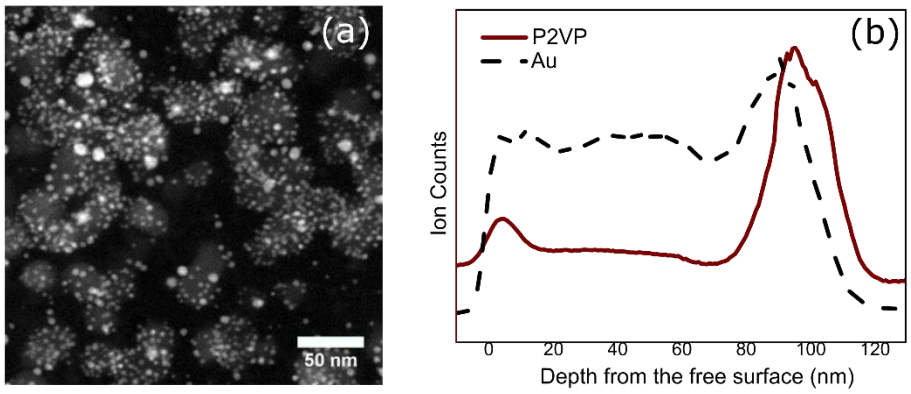

Figure 5 - 1. (a) STEM image and (b) DSIMS depth profiles of Au and P2VP in PS-b-P2VP/PS mixtures contaianing 20 wt% PS(N=10)-Au(d≈4 nm)

The study in chapter 4 shows that the phase behaviors of thin film BCP/star-shaped polymer blends (BCP is the minor component) can be tuned by the number of arms, *f* and arm length, N_{arm} of star-shaped polymer. Miscibility or phase separation of micelles is readily achieved in this system. In addition, phase separated micelles form close-packed structures. It would then be desirable to establish the phase diagram of this system by progressively changing *f* and N_{arm}. Meanwhile, one can explore morphological behaviors of BCP/star-shaped polymer mixtures with low concentration of star-shaped polymers. The results could be compared with morphologies of brush coated NP/BCP systems as a function of grafting density ∑ and grafted chain length N since the structure of polymer grafted NPs start resembling that of a star-shaped molecule when $R < N^{1/2}a$. Note that ∑ and N of NPs can be considered equivalent to f and N_{arm} of star-shaped molecules, respectively. In addition, wetting experiments of star-shaped molecules on the BCP brush layer coated substrate could be examined to determine the wetting-dewetting transition. From these suggested

experiments, we could gain a deeper understanding of thermodynamic interactions between star-shaped molecules and BCPs and thus obtain desired surface properties or other physical properties on demand.

APPENDICES

Appendix A. Supplemental Information for Chapter 2

All samples used in this work were annealed above T_g for 4 hours, here we do time evoluted annealing study using the sample of AuNPs in thin film PS-b-P2VP/PS mixtures (weight ratio of 1:4) with host PS degree of polymerization P=15400 to determine if our films were in equilibrium condition. Please note that sample with P=15400 should have the highest viscosity and will spend the longest time to reach equilibrium condition compared to other samples used in our work (P=125, P=1460 and P=5660).

Based on the organization of micelles and nanoparticles within the films as shown below, the micelles were fully developed within annealing of 4 hours and size distribution of micelles did not change with further annealing even after two days. It is considered that our samples are in equilibrium.

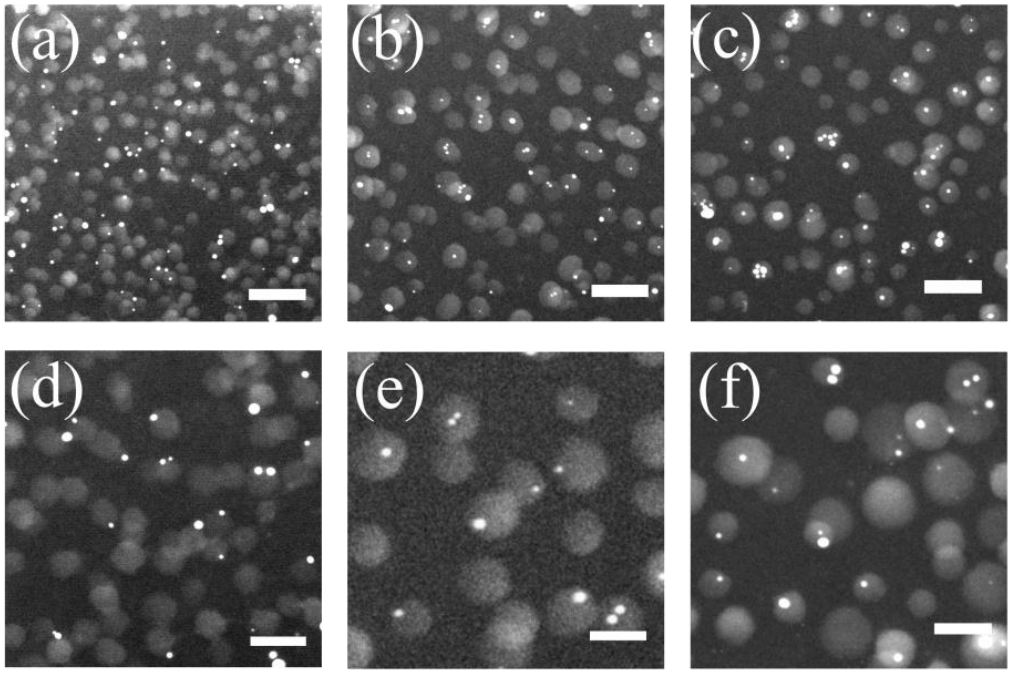

Figure S - 1. Scanning transmission electron micrographs (STEM) of AuNPs in thin film PS-b-P2VP/PS mixtures (weight ratio of 1:4) with host PS degrees of polymerization P=15400 (a,d) as cast sample (b,e) annealed above Tg for 4 hours and (c,*f*) annealed above Tg for 48 hours. The scale bar represents a distance of 100nm in (a-c) and it represents 50nm in (d-*f*).

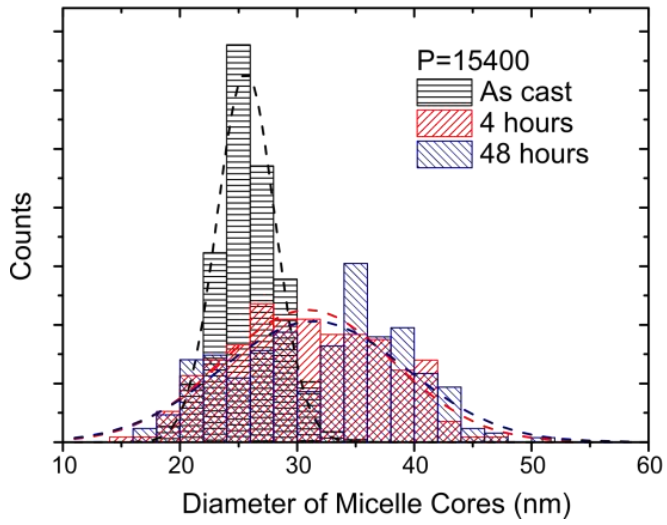

Figure S - 2. Histograms of diameter of all micelle cores for as cast sample, samples annealed for 4 hours and 48 hours as determined from STEM images. The size distributions of micelle cores for these three samples are fitted to Gaussian profile.

Table S - 1. Quantitative comparison of AuNPs in thin film PS-b-P2VP/PS mixture with P=15400 among as cast sample and annealed samples (4 hours and 48 hours)

	Diameter of Micelles (nm)	Number Density of Micelles (μm^{-3})	Volume Fraction of Micelles	Fraction of Micelles with AuNPs
As cast	25.8 ± 2.6	6.0 ± 0.3x10^3	0.154 ± 0.009	N.A.
4 hours	30.8 ± 6.4	2.9 ± 0.2x10^3	0.136 ± 0.013	0.46 ± 0.13
48 hours	31.9 ± 7.2	2.5 ± 0.2x10^3	0.139 ± 0.017	0.49 ± 0.05

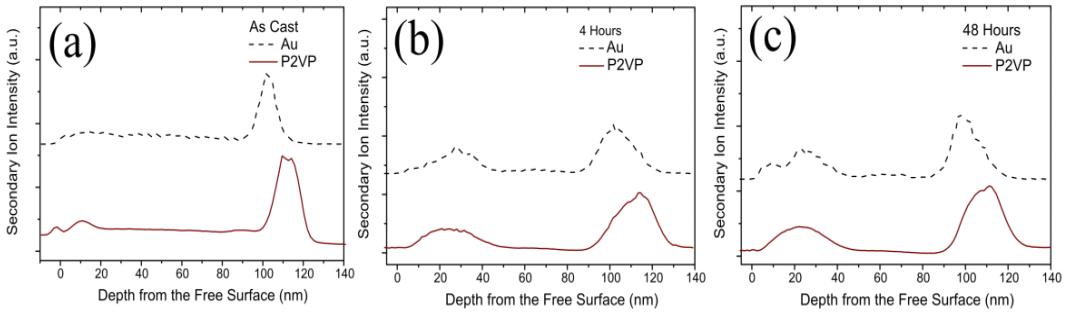

Figure S - 3. Depth profiles of AuNPs and of the P2VP in AuNPs/polymer blend with P=154000 (a) as cast (b) annealed for 4 hours and (c) annealed for 48 hours

Appendix B. Supplemental Information for Chapter 3

Calculation of Nanoparticle Projection:

This calculation follows that of Mai et al.[1] In this model, it is assumed that nanoparticles are evenly distributed at the surface of a sphere. Our calculation is performed using a hemispherical geometry, for simplicity. Because the system is symmetric, the results would be representative of the behavior of a spherical system. In Figure S - 4, nanaoparticles on the surface of the hemisphere between the equator and the direction of the angle= 90°- α (AB belt) will project on the shaded area of the equatorial plane. The fractional percent of nanoparticles projected on the shaded area, p, is equivalent to the surface area ratio of the AB belt to that of the hemisphere, as expressed in the following:

$$\mathrm{p} = \frac{S_{AB}}{S_{hemisphere}} = cos\alpha \qquad (1)$$

cos(α) may be expressed in terms of R and L, where R and L are defined in Figure S - 4:

$$\cos\alpha = \frac{\sqrt{R^2 - OC^2}}{R} = \sqrt{1 - (1 - \frac{L}{R})^2} \qquad (2)$$

After combining equation (1) and (2), we obtain an expression for p as a function of L/R, where 0≤L/R≤1:

$$p = \sqrt{1 - (1 - \frac{L}{R})^2} \qquad (3)$$

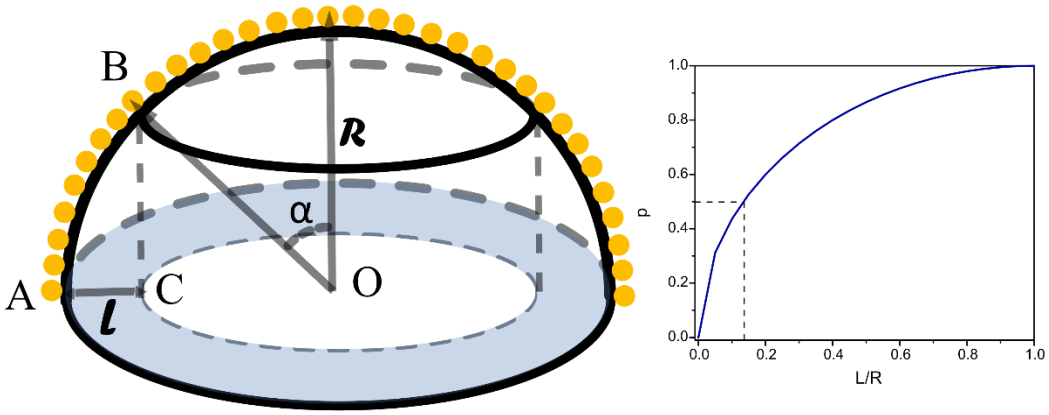

Figure S - 4. A model is used to derive the theoretical equation (3) (left schematic) and the plot of equation (3) shows that most nanoparticles are projected at the inner edge of the perimeter of the equator when they are on the surface of a sphere (right plot).

Calculation of van der Waals Interaction Energy:

In this multi-layer model, the PS coated gold nanoparticle is considered to be a sheathed sphere. The free surface and the Si_3N_4 substrate are treated as infinite slabs. The interaction energy between the sheathed sphere and the infinite slab is given as following equation: [2,3]

$$G_{vdW} = -[A_{PS-M-S}H(x_{11}) + (A_{Au-M-S} - A_{PS-M-S})\mathrm{H}(x_{12})] \quad (4)$$

$$\mathrm{H}(x_{ij}) = \frac{1}{12}\left(\frac{1}{x_{ij}} + \frac{1}{x_{ij}+1} + 2ln\frac{x_{ij}}{x_{ij}+1}\right) \quad (5)$$

$$x_{11} = \frac{L_{NP-Slab}}{d_{Au}}\,;\, x_{12} = \frac{L_{NP-Slab}+h}{d_{Au}} \quad (6)$$

Parameters used in equation (4-6) are defined in Figure S - 5. A is the Hamaker constant. The subscripts PS, M, S and Au of A represent the grafted PS layer, polymer blend medium, slab and gold respectively. The Hamaker constant of A_{123} (interaction of

component 1 and component 3 across the medium 2) can be estimated from the Hamaker constant of the pure component as follow:[4]

$$A_{123} = (\sqrt{A_{11}} - \sqrt{A_{22}})(\sqrt{A_{33}} - \sqrt{A_{22}}) \quad (7)$$

Where $A_{PS\text{-}PS}$=6.5, $A_{Au\text{-}Au}$=40, $A_{Si3N4\text{-}Si3N4}$=17 are obtained from the literature and the Hamaker constant of polymer blend medium can be estimated from equation (8),[4]

$$A_{M-M} = [\varphi_{PS}\sqrt{A_{PS-PS}} + (1-\varphi_{PS})\sqrt{A_{P2VP-P2VP}}]^2 \quad (8)$$

$$A_{P2VP-P2VP} \approx 2.1 \times 10^{-21}\gamma \quad (9)$$

Where the surface energy of P2VP γ =46.7 dyn/cm^2.[5] From equation (8) and (9), $A_{M\text{-}M}$= 6.55.

The Hamaker constant of supercritical CO_2 can be obtained from equation (10),

$$A_{11} = \frac{3}{4}kT\left(\frac{\varepsilon_1-1}{\varepsilon_1+1}\right)^2 + \frac{3h\upsilon_e}{16\sqrt{2}}\frac{(n_1{}^2-1)^2}{(n_1{}^2+1)^{\frac{3}{2}}} \quad (10)$$

Here the static dielectric constant ε=1.39 and refractive index n=1.15 for supercritical CO_2 at 50°C and 13.8MPa.[6] The absorption frequency υ_e=2×10^{15} s^{-1}.

Based on the above equations, the nonretarded long-range van der Waals interaction energy between PS-coated nanoparticle and the substrate or the free surface at the presence of supercritical CO_2 has been calculated and shown in Figure 3 - 7e.

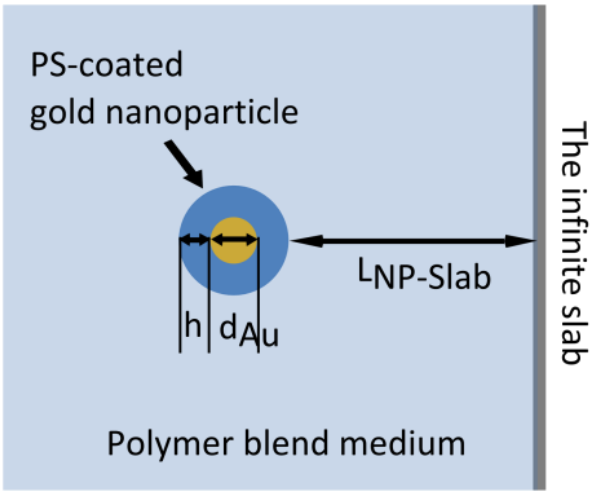

Figure S - 5. Illustration of the multi-layer model used in the calculation. h represents the thickness of grafted PS layer on the particle; d_{Au} is the core diameter of gold nanoparticle and L_{NP}-Slab is the distance between PS-coated nanoparticle and the infinite slab

Morphology of Pure Polymer Blend (P < N_{PS}, "Wet-brush" Micelles):

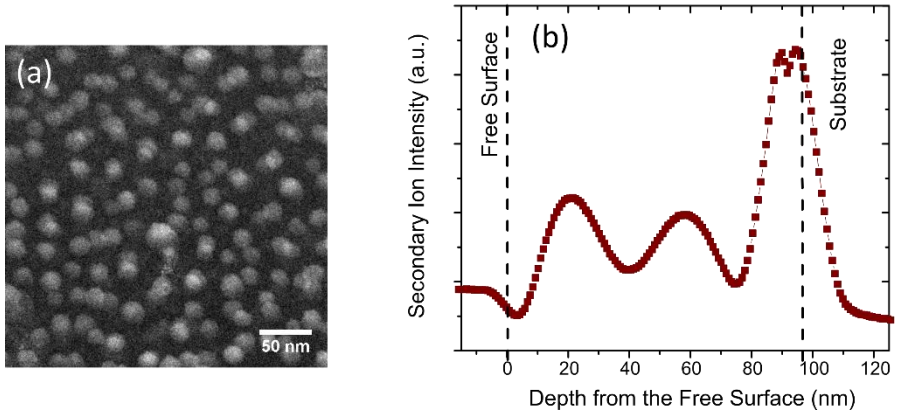

Figure S - 6. (a) An STEM image of the P2VP cores of micelles in a PS-b-P2VP/PS(P=125) mixture (weight ratio of copolymer to homopolymer is 1:4). The sample was annealed in supercritical CO2 at 50 oC, at a pressure of 13.8 MPa for 24 hours (under these conditions the sample is mildly plasticized in order to impart the system sufficient mobility). (b) The DSIMS image of the depth profile (CN) of P2VP is shown

The STEM image in Figure S3a shows spherical micelles in the PS (P=125) after $scCO_2$ annealing. The P2VP cores, of average diameter 18 nm appear bright in the images due to staining by iodine vapor. As discussed in earlier publication,[7,8] when $P < N_{PS}$ the short host chains readily intermix with the micelle coronas, this is so called "wet-brush" micelle condition. As a result of intermixing, the PS coronas are stretched and the P2VP cores are concurrently compressed in order to maintain a constant segmental density. Compared to the "dry-brush" condition ($P \gg N_{PS}$), this "wet brush" condition favors the formation of smaller micelles because it maximizes the extent of intermixing between the host and corona chains. The micelles are more uniformly distributed throughout the sample in order to enhance translational entropy of the system, which is evident from DSIMS in Figure S - 6b.

References

(1) Mai, Y.; Eisenberg, A. *J. Am. Chem. Soc.* **2010**, *132*, 10078.
(2) Nir, S. *Prog. Surf. Sci.* **1977**, *8*, 1.
(3) Meli, L.; Li, Y.; Lim, K. T.; Johnston, K. P.; Green, P. *F. Macromolecules* **2007**, *40*, 6713.
(4) Israelachvili, J. N. In *Intermolecular and Surface Forces, 3rd ed.*; Israelachvili, J. N., Ed.; Academic Press: San Diego, 2011, p 253.
(5) Sauer, B. B.; Dee, G. T. *Macromolecules* **2002**, *35*, 7024.
(6) Obriot, J.; Ge, J.; Bose, T. K.; St-Arnaud, J. M. *Fluid Phase Equilibria* **1993**, *86*, 314.
(7) Chen, X. C.; Yang, H. X.; Green, P. *F. Macromolecules* **2011**, *44*, 5758.
(8) Zhao, J.; Chen, X. C.; Green, P. *F. Soft Matter* **2013**, *9*, 6128.